45. Wu Y, Wan T, Zhou X, Wang B, Yang F, Li N, Chen G, Dai S, Liu S, Zhang M, Cao X: **Hsp70-like protein I fusion protein enhances induction of carcinoembryonic antigen-specific CD8+ CTL response by dendritic cell vaccine.** *Cancer Res* 2005, **65**:4947-4954.

(page number not for citation purposes)

Identification of an Immunogenic CTL Epitope of HIFPH3 for Immunotherapy of Renal Cell Carcinoma

Eiji Sato,[1] Toshihiko Torigoe,[2] Yoshihiko Hirohashi,[2] Hiroshi Kitamura,[1] Toshiaki Tanaka,[1] Ichiya Honma,[1] Hiroko Asanuma,[3] Kenji Harada,[4] Hideo Takasu,[4] Naoya Masumori,[1] Naoki Ito,[1] Tadashi Hasegawa,[3] Taiji Tsukamoto,[1] and Noriyuki Sato[2]

Abstract

Purpose: CD8^{+} CTLs have an essential role in immune response against tumor. Although tumor-associated antigens have been identified in renal cell carcinoma (RCC), few of these are commonly shared and investigated as therapeutic targets in the clinical medicine. In this report, we show that HIFPH3, a member of prolyl hydroxylases that function as oxygen sensor, is a novel tumor antigen and HIFPH3-specific CTLs are induced from peripheral blood lymphocytes of RCC patients.

Experimental Design: Expression of HIFPH3 was examined by reverse transcription-PCR and immunostaining with anti-HIFPH3 antibody. To identify HLA-A24-restricted T-cell epitopes of HIFPH3, eight peptides were selected from the amino acid sequence of this protein and screened for their binding affinity to HLA-A24. Peptide-specific CTLs were induced by stimulating peripheral blood lymphocytes of HLA-A24-positive RCC patients with these peptides *in vitro*. HLA-A24-restricted cytotoxicity of the CTLs against HIFPH3^{+} RCC lines was assessed by chromium release assay.

Results: HIFPH3 was overexpressed in many RCC cell lines and primary RCC tissues, whereas it was not detectable in normal adult tissues by reverse transcription-PCR. Of the eight peptides that contained HLA-A24-binding motif, HIFPH3-8 peptide (amino acid sequence, RYAMTV-WYF) could induce the peptide-specific CTLs from 3 of 6 patients with HIFPH3-positive RCC. Furthermore, HIFPH3-8 peptide-specific CTLs showed cytotoxicity against HIFPH3^{+} RCC cell lines in a HLA-A24-restricted manner.

Conclusions: HIFPH3 may be a target antigen in immunotherapy for RCC and HIFPH3-8 peptide could be used as a peptide vaccine for HLA-A*2402[+]/HIFPH3^{+} RCC patients.

Surgery is the only known effective therapy for localized renal cell carcinoma (RCC); however, ~ 20% of all patients surgically treated with curative intent will ultimately experience disease recurrence (1) and ~ 30% of patients will present metastatic disease. Although systemic therapy with radiation and/or chemotherapeutic drugs is applied for locally advanced or metastatic RCC, its efficacy is limited due to the resistance to the therapy. Nonspecific immunotherapy with IFN-α and/or

interleukin (IL)-2 has been also established as the primary therapy for metastatic RCC. However, neither agent provides substantial clinical benefit in the majority of patients. The number of durable responses is limited, and the use of these agents is complicated due to the significant safety and tolerability issues (2, 3). Hence, there is great need for new strategies of target-specific immunotherapy for the treatment of RCC, and recent progress in understanding of tumor immunology has raised expectations that specific immunotherapy may become a new modality of cancer therapy. Since the establishment of methods to isolate genes encoding tumor antigens that were recognized by CTLs, numerous tumor-associated antigens have been identified in melanoma and various other types of cancer (4, 5). Although tumor-associated antigens have been also identified in RCC, few of these are commonly shared and can be studied for clinical applications (6–9). There are no RCC-associated antigens currently being investigated as immunotherapeutic targets of RCC in clinical trials.

Tumor progression is highly regulated by hypoxia, a low level of oxygen, which occurs after excessive tumor cell proliferation that distances cells from oxygen-rich blood vessels. A consequence of increased cell number within a tumor is a corresponding increase in oxygen consumption. The hypoxia-inducible factor-1 (HIF-1), a transcriptional complex composed of an oxygen-sensitive α-subunit and a β-subunit, is the most

Translational Relevance

Although systemic therapy with radiation and/or chemotherapeutic drugs is applied for locally advanced or metastatic RCC, its efficacy is limited due to the resistance to the therapy. Nonspecific immunotherapy with IFN-α and/or interleukin-2 has been also established as the primary therapy for metastatic RCC. However, neither agent provides substantial clinical benefit in the majority of patients. Hence, there is great need for new strategies of target-specific immunotherapy for the treatment of RCC, and recent progress in understanding of tumor immunology has raised expectations that specific immunotherapy may become a new modality of cancer therapy. In the present article, we showed that HIFPH3 was one of potent immunogenic antigens of RCC and that HIFPH3-8 peptide might serve as a tumor vaccine for HLA-A*2402+ RCC patients. It is expected that HIFPH3 targeting immunotherapy might become a rational modality in therapy for RCC.

important factor involved in the cellular response to hypoxia. Overexpression of the HIF-1 subunit, resulting from intratumoral hypoxia and genetic alterations, has been shown in common human cancers and is correlated with tumor angiogenesis and patient mortality. Under normoxia, HIF-1 is continuously expressed in the cell but immediately degraded via the proteasomal pathway after ubiquitination (10). The von Hippel-Lindau (VHL) protein acts as a particle recognition protein of the responsible E3 ubiquitin-ligase complex if two distinct prolyl residues within a region, referred to as the oxygen-dependent degradation domain of HIF-1, Pro^{402}, and/or Pro^{564}, are hydroxylated (11–15). The site-specific hydroxylation of HIF prolyl residues is catalyzed by a conserved class of 2-oxoglutarate-dependent and Fe (II)-dependent dioxygenases, designated HIF prolyl hydroxylases (HIFPH; refs. 15–18). Three different HIFPHs, HIFPH1, HIFPH2, and HIFPH3, have been identified, but the difference among their *in vivo* roles remain unclear. Some studies have pointed out that HIFPH3 is strikingly expressed by hypoxia, displays high substrate specificity, and has been identified in other signaling pathways. HIFPH3 may therefore hydroxylate divergent substrates and/or connect divergent cellular responses with HIF (19).

In this report, we focused on the characteristics of HIFPH3 as a novel tumor antigen. We show that HIFPH3 expression was detected in certain RCC cell lines and primary RCC tissues by reverse transcription-PCR (RT-PCR) and immunohistochemical staining. However, its expression could not be detected in normal adult tissues by the most sensitive RT-PCR method. We identified several 9- or 10-mer peptides with HLA-A24-binding motif derived from HIFPH3 protein, and some of the peptides had relatively high binding affinity to HLA-A24 molecule. By stimulating peripheral blood mononuclear cells (PBMC) from HLA-A*2402+/HIFPH3+ RCC patients with HIFPH3 peptides, CTLs specific for HIFPH3-8 peptide could be successfully induced. In addition, CTLs induced by HIFPH3-8 peptide were capable of exerting cytotoxicity on HIFPH3+ RCC cell line in a HLA-A24-restricted manner. These data highlight HIFPH3 as a

potent target for immunotherapy of RCC and raise the possibility that HIFPH3-8 peptide may be suitable for the peptide-based vaccine for HLA-A*2402+ RCC patients.

Materials and Methods

Patients and samples. The surgically resected tissue specimens and PBMC used in this study were obtained from HLA-A*2402+ RCC patients who were hospitalized at Sapporo Medical University Hospital after obtaining their informed consent. PBMCs of RCC patients were obtained just before the nephrectomy and prepared for the CTL induction freshly without cryopreservation.

Cell lines and culture media. RCC cell lines SMKT R-1 (HLA-A*2402+), SMKT R-2 (HLA-A*2402+), SMKT R-3 (HLA-A*2402-), and SMKT R-4 (HLA-A*2402-), lung cancer line LHK2, gastric cancer line SSTW, and pancreatic cancer line PUN were established in our laboratory. RCC cell lines Caki-1 (HLA-A*2402+), ACHN (HLA-A*2402-), melanoma lines 888MEL and LG2MEL, colon cancer line SW450, lung cancer lines LNY-1, A549, 1-87, and LK79, pancreas cancer line HS776T, hepatic cancer line CHC20, and erythroleukemia cell line K562 were purchased from the American Type Culture Collection. All these cell lines were cultured in RPMI 1640 (Sigma) or DMEM (Sigma) supplemented with 10% fetal bovine serum (Filtron). SMKT R-4*2402, a stable transfectant of HLA-A*2402 cDNA of SMKT R-4 cells was cultured in RPMI 1640 supplemented with 10% fetal bovine serum and 500 ng/mL puromycin (Sigma). T2-A*2402, a stable transfectant of HLA-A*2402 cDNA of T2 cells (a kind gift from Dr. K. Kuzushima, Aichi Cancer Research Institute), was cultured in RPMI 1640 supplemented with 10% fetal bovine serum and 800 μg/mL G418 (Invitrogen Life Technologies).

Development of monoclonal anti-HIFPH3 antibody. Monoclonal antibody against HIFPH3 was generated by immunizing mice eight times every week with recombinant His-tag HIFPH3 protein, which was produced and purified by Ni-NTA agarose column (Qiagen) as described previously (20). Spleen cells were fused with NS-1 myeloma cells by using polyethylene glycol 4000 (Kanto Kagaku) and plated into 96-well plates. Hybridoma supernatants were initially screened using an ELISA with recombinant His-HIFPH3 protein and then screened by Western blotting. The third screening of the supernatants was done by immunostaining of formalin-fixed, paraffin-embedded human tissue sections. The resulting hybridoma EMR-PHD3 was cloned by limiting dilution and finally its subclone EMR-PHD3-7 that produced monoclonal anti-HIFPH3 antibody with IgG1 subclass and κ chain was established.

Immunohistochemical staining of tissue sections. Immunohistochemical staining was done with formalin-fixed, paraffin-embedded sections of surgically resected tumor specimens of RCCs. Sections (4-5 μm thick) were deparaffinized in xylene and rehydrated in graded alcohols. Antigen retrieval was done by boiling sections for 20 min in a microwave oven in preheated 0.01 mol/L sodium citrate (pH 6.0). Endogenous peroxidase activity was blocked by 3% hydrogen peroxide in ethanol for 10 min. After blocking with 1% nonfat dry milk in PBS (pH 7.4), the sections were reacted with monoclonal anti-HIFPH3 antibody EMR-PHD3-7 for 1 h followed by incubation with biotinylated anti-mouse IgG (Nichirei) for 30 min. Subsequently, the sections were stained with streptavidin-biotin complex (Nichirei), followed by incubation with 3,3'-diaminobenzidine used as the chromogen and counterstaining with hematoxylin.

RT-PCR analysis. Multiple tissue cDNA panels (BD Biosciences Clontech) were used as a template of normal tissue cDNA. Total RNA was isolated from cultured cells and tumor tissues by using ISOGEN reagent (Nippon Gene). cDNA mixture was synthesized from 1 μg total RNA by reverse transcription using SuperScript II and oligo(dT) primer (Invitrogen Life Technologies) according to the manufacturer's protocol. PCR amplification was done in 50 μL PCR mixture containing 1 μL cDNA mixture, 1 μL KOD Plus DNA polymerase (Toyobo), and

— 279 —

15 pmol primers. The PCR mixture was initially incubated at 94°C for 2 min followed by 35 cycles of denaturation at 94°C for 15 s, annealing at 64°C for 30 s, and extension at 72°C for 30 s. For specific detection of HIFPH3, the primer pairs 5'-CATCCCTGTCTTGTGTGTGG-3' and 5'-CCAACAGCCCTGGATTAAGA-3' were employed as forward and reverse primers, respectively. The expected size of PCR product for HIFPH3 is 420 bp. For an internal control, glyceraldehyde 3-phosphate dehydrogenase expression was detected by using forward primer 5'-ACCACAGTCCATGCCATCAC-3' and reverse primer 5'-TCCACCAC-CCTGTTGCTGTA-3' with an expected PCR product of 452 bp. The PCR products were visualized with ethidium bromide staining under UV light following electrophoresis on 1.0% agarose gel. The nucleotide sequence of the PCR products was confirmed by direct sequencing using an ABI Genetic Analyzer PRISM 310 and an AmpliCycle sequencing kit (Perkin-Elmer).

Peptides and cytokines. HIFPH3-derived peptides carrying HLA-A24-binding motif HIFPH3-1 (IMRLDLEKI), HIFPH3-2 (NWDAKLHGGI), HIFPH3-3 (IFPEGKSFI), HIFPH3-4 (SFIADVEPI), HIFPH3-5 (GFCYLDNFL), HIFPH3-6 (SFLLSLIDRL), HIFPH3-7 (YYVKERSKAM), HIFPH3-8 (RYAMTVWYF), EBV LMP2-derived HLA-A24-binding peptide (TYGPVFMSL; ref. 21), and HIV env-derived HLA-A24-binding peptide (RYLRDQQLLGI; ref. 22) were purchased from Greiner Bio-One. The peptides were dissolved in DMSO at the concentration of 5 mg/mL and stored at -80°C. Human recombinant IL-2, IL-4, and granulocyte-macrophage colony-stimulating factor were kind gifts from Takeda Pharmaceutical, Ono Pharmaceutical, and Novartis Pharmaceutical, respectively. Human recombinant IL-7 was purchased from Invitrogen Life Technologies.

Peptide binding assay. Peptide binding affinity to HLA-A24 molecule was assessed by HLA-A24 stabilization assay as described previously (22) based on the findings that MHC class I molecules could be stabilized on the cell surface in the presence of binding peptides. T2-A*2402 cells are the peptide transporter-negative B/T hybrid cell line 174 CEM.T2 (referred to as T2) transfected with a plasmid expressing HLA-A*2402. After incubation of T2-A*2402 cells in culture medium at 26°C for 18 h, 2×10^5 cells were washed with PBS and suspended with 1 mL Opti-MEM (Life Technologies) with or without 100 µg peptide followed by incubation at 26°C for 3 h and then at 37°C for 2.5 h. After washing with PBS, the cells were

incubated with anti-HLA-A24 monoclonal antibody at 4°C for 1 h followed by incubation with FITC-conjugated rabbit anti-mouse IgG at 4°C for 30 min. The cells were then suspended with 1 mL PBS containing 1% formaldehyde and analyzed by FACScan (Becton Dickinson). Binding affinity was evaluated by comparing mean fluorescence intensity (MFI) of HLA-A24 expression in the presence of peptide pulsation.

Peptide-specific CTL induction with immature dendritic cells and phytohemagglutinin blasts. CTLs were induced from PBMCs of cancer patients by using autologous dendritic cells and phytohemagglutinin (PHA) blasts as antigen-presenting cells (APC; refs. 23, 24). Briefly, PBMCs (1×10^7-1×10^8) were isolated from blood of cancer patients by using Lymphoprep (Nycomed) and then separated into CD14+ and CD14- cells by using MACS separation system (Miltenyi Biotech) and anti-CD14 monoclonal antibody coupled with magnetic microbeads according to the manufacturer's instruction. Autologous immature dendritic cells were generated from CD14+ cells in the plastic flask by culturing in AIM-V medium supplemented with 10% human serum, 10 mmol/L HEPES, 50 µmol/L 2-mercaptoethanol, 100 ng/mL granulocyte-macrophage colony-stimulating factor, and 1,000 units/mL IL-4 for 7 days. CD8+ cells were isolated from CD14- cells by using MACS separation system and anti-CD8 monoclonal antibody coupled with magnetic microbeads according to the manufacturer's instruction. PHA blasts were derived from CD14-CD8- cells by culturing in AIM-V medium supplemented with 10 mmol/L HEPES, 50 µmol/L 2-mercaptoethanol, 100 units/mL IL-2, and 1 µg/mL PHA for 2 days followed by culture in AIM-V medium without PHA for 5 days. APCs (dendritic cells and PHA blasts) were cultured in AIM-V medium supplemented with 50 µmol/L peptide at room temperature for 2 h followed by washing with AIM-V medium once and then irradiated (100 Gy) and used for stimulation of CTL. CTL induction procedure was initiated by stimulating CD8+ cells with peptide-pulsed autologous dendritic cells at a 20:1 effecter/APC ratio in AIM-V medium supplemented with HEPES, 2-mercaptoethanol, and 10 ng/mL IL-7 for 7 days at 37°C. The following stimulation was done with peptide-pulsed PHA blasts at a 10:1 effector/APC ratio. On the next day of the second stimulation, IL-2 was added to the culture at a concentration of 10 units/mL. The same CTL stimulation cycle with PHA blasts was then done twice more over the period of 2 weeks. One week after
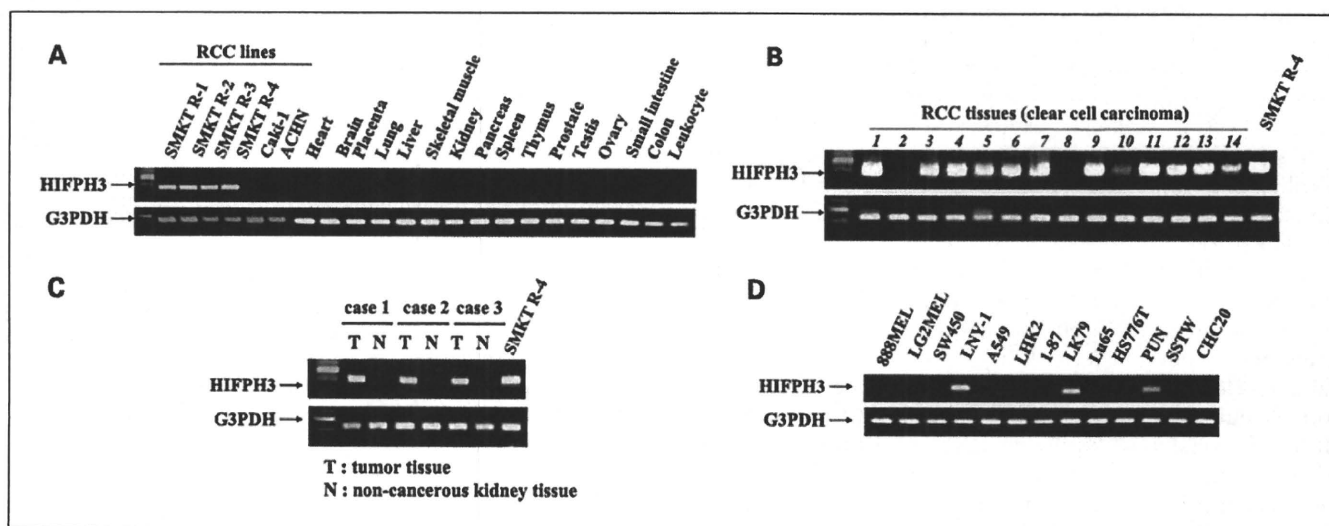
Fig. 1. Expression profiles of HIFPH3 as assessed by RT-PCR in normal adult tissues, RCC cell lines, and primary RCC tissues. *A,* expression of HIFPH3 in RCC cell lines and normal tissues including heart, brain, placenta, lung, liver, skeletal muscle, kidney, pancreas, spleen, thymus, prostate, testis, ovary, small intestine, colon, and leukocyte. Glyceraldehyde 3-phosphate dehydrogenase expression was detected as an internal control. *B,* expression of HIFPH3 in primary RCC tissues. *C,* expression of HIFPH3 in RCC tumor tissue (*T*) and noncancerous tissue (*N*) of 3 RCC cases. *D,* expression of HIFPH3 in various tumor cells including melanoma lines 888MEL and LG2MEL, colon cancer line SW450, lung cancer lines LNY-1, A549, LHK2, 1-87, LK79, and Lu65, pancreatic cancer lines HS776T and PUN, gastric cancer line SSTW, and hepatic cell cancer line CHC20.

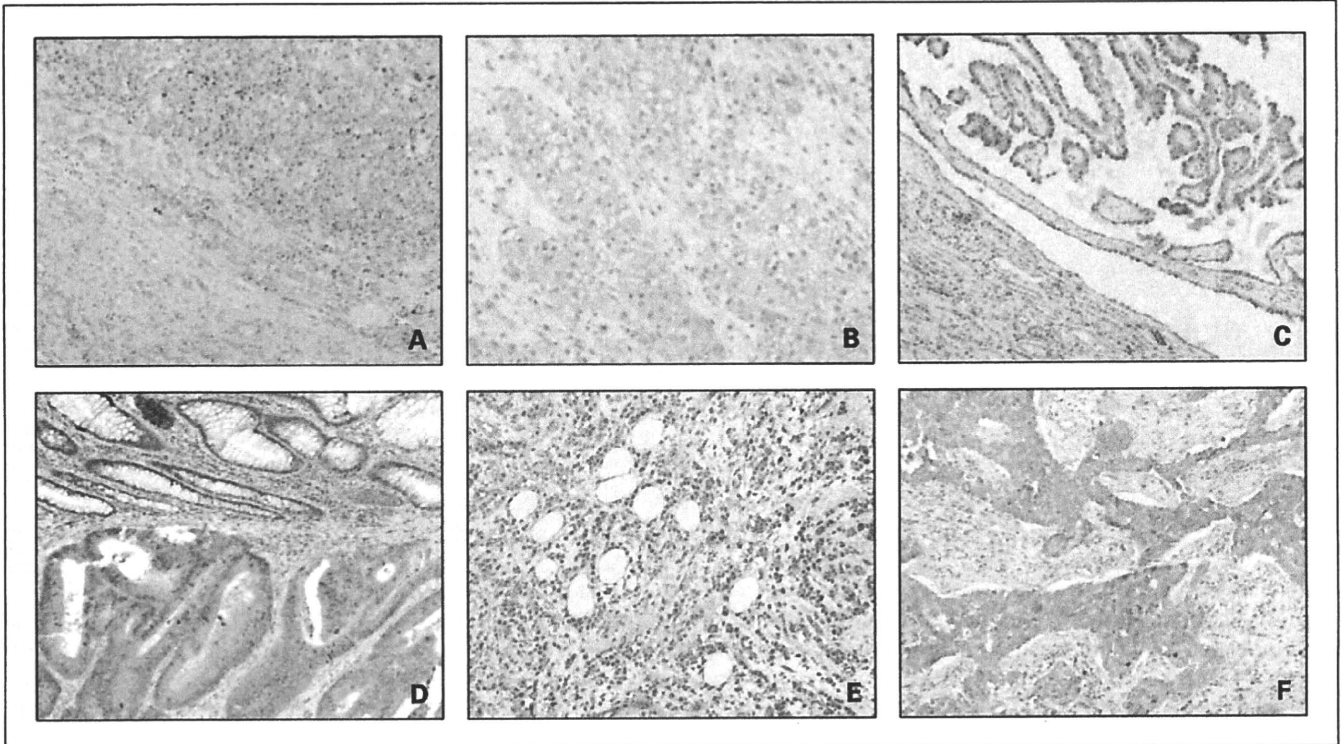**Fig. 2.** Immunohistochemical staining of HIFPH3 in RCC and other types of tumors. *A*, low magnified view (×40) of clear cell RCC. *B*, high magnified view (×100) of clear cell RCC. *C*, low magnified view (×40) of papillary RCC. *D*, low magnified view (×40) of colon cancer tissue. *E*, low magnified view (×40) of breast cancer tissue. *F*, low magnified view (×40) of lung cancer tissue.

the fourth stimulation, cytotoxic activity of the CTL was measured by ^{51}Cr release assay.

Cytotoxicity assay. The cytotoxic activities of CTLs were measured by ^{51}Cr release assay as described previously (25). Briefly, target cells were labeled with 100 μCi ^{51}Cr for 1 h at 37°C and washed with RPMI 1640 thrice. Then, 2×10^3 ^{51}Cr-labeled target cells were incubated with effecter cells at various E:T ratios at 37°C for 6 h in V-bottomed 96-well microtiter plates. Then, supernatants were collected and the radioactivity was measured with a γ-counter. % Specific lysis was calculated as follows: % specific lysis = (test sample release - spontaneous release) × 100 / (maximum release - spontaneous release). For preparation of peptide-pulsed target cells, target cells were incubated with 100 μg/mL peptide at room temperature for 1 h before the assay.

Results

HIFPH3 is expressed in RCC cell lines and primary RCC tissues but not in normal adult tissues. In this report, HIFPH3 expression profiles in normal adult tissues and RCC cell lines and tissues were analyzed by RT-PCR method. We first studied HIFPH3 expression in RCC cell lines and normal adult tissues including heart, brain, placenta, lung, liver, skeletal muscle, kidney, pancreas, spleen, thymus, prostate, testis, ovary, small intestine, colon, and leukocyte. As shown in Fig. 1A, HIFPH3 mRNA was detected in 4 of 6 RCC cell lines (SMKT R-1, R-2, R-3, and R-4). Nucleic acid sequence of the HIFPH3-specific band was confirmed by DNA sequence analysis (data not shown). In contrast, no overt expression of HIFPH3 mRNA was observed in these normal adult tissues on the condition of detecting the expression of glyceraldehyde 3-phosphate dehydrogenase mRNA. These data indicate that HIFPH3 is aberrantly expressed in certain RCC cell lines. We then analyzed the

HIFPH3 expression in primary RCC tissue specimens. As shown in Fig. 1B, the expression of HIFPH3 was detected in certain RCC tissues in 13 of 15 (87%) cases. These data indicate that HIFPH3 was expressed in primary RCC tissues as well as in RCC cell lines.

We then examined the expression of HIFPH3 in cancerous tissue and noncancerous tissue of 3 RCC cases (Fig. 1C). HIFPH3 was selectively expressed in cancerous tissue but not in noncancerous tissue.
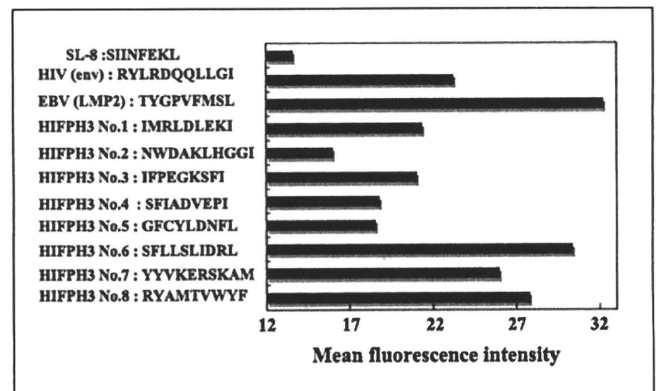
Fig. 3. Amino acid sequences of HIFPH3-derived peptides with HLA-A24-binding motif and their binding assay to HLA-A24 molecule. Eight peptides carrying HLA-A24-binding motif (HIFPH3-1-HIFPH3-8) were synthesized. Binding affinity of HIFPH3-derived peptides to HLA-A24 molecule was evaluated by MFI of cell surface HLA-A24 molecule on T2-A*2402 cells that were pulsed with each peptide. HLA-A24-bound EBV LMP2-derived peptide (*TYGPVFMSL*) and HIV env-derived peptide (*RYLRDQQLLGI*) were used as positive controls. SL-8 peptide (*SIINFEKL*) was used as a negative control. Histograms of MFI were displayed for each peptide.

— 281 —

Table 1. Summary of clinicopathologic characteristics and peptide-reactive CTL induction from PBMCs of HIFPH3$^+$ clear cell carcinoma patients

Case no.	Age	Sex	Stage*	Peptides	HLA-A*2402	CTL induction †
1	56	M	$T_{1a}N_0M_0$	HIFPH3-8	+	+
2	54	F	$T_{1b}N_0M_0$	HIFPH3-8	+	+
3	72	M	$T_{1a}N_0M_0$	HIFPH3-8	+	+
4	68	F	$T_{1b}N_0M_0$	HIFPH3-8	+	-
5	50	M	$T_{1a}N_0M_0$	HIFPH3-8	+	-
6	56	M	$T_{1a}N_0M_0$	HIFPH3-8	+	-
7	61	F	$T_{1a}N_0M_0$	HIFPH3-1 to HIFPH3-4	+	-
8	65	M	$T_{1a}N_0M_0$	HIFPH3-1 to HIFPH3-4	+	-
9	53	M	$T_{1a}N_0M_0$	HIFPH3-5 to HIFPH3-8	+	-
10	75	M	$T_{1a}N_0M_0$	HIFPH3-5 to HIFPH3-8	+	+
11	68	F	$T_{1b}N_0M_0$	HIFPH3-8	-	-
12	82	M	$T_{1a}N_0M_0$	HIFPH3-8	-	-

*Tumor-node-metastasis classification.
†<20% specific lytic activity against HIFPH3 peptide-pulsed T2-A*2402 target cells was indicated as +.

To know if HIFPH3 is expressed in non-RCC tumor cells, various tumor cells were examined by RT-PCR, including melanoma lines, lung cancer lines, colon cancer line, pancreatic cancer line, gastric cancer line, and hepatic cell cancer line. Of these tumor cells, two of lung cancer lines and one of pancreatic cancer lines had expression of HIFPH3 (Fig. 1D).

Immunohistochemical staining of HIFPH3. To detect the HIFPH3 protein expressed in RCC tissues, we generated HIFPH3-specific monoclonal antibody suitable for immunohistochemical staining. HIFPH3-specific reactivity of the antibody was confirmed by Western blotting (data not shown). Representative pictures of RCC tissue staining are shown in Fig. 2A to C, indicating cytoplasmic staining of HIFPH3 in RCC cells. Of 18 cases of clear cell RCC, 13 (72%) cases were HIFPH3 positive by immunostaining (Fig. 2A and B). In contrast, only 3 of 9 (33%) cases of non-clear cell RCC were
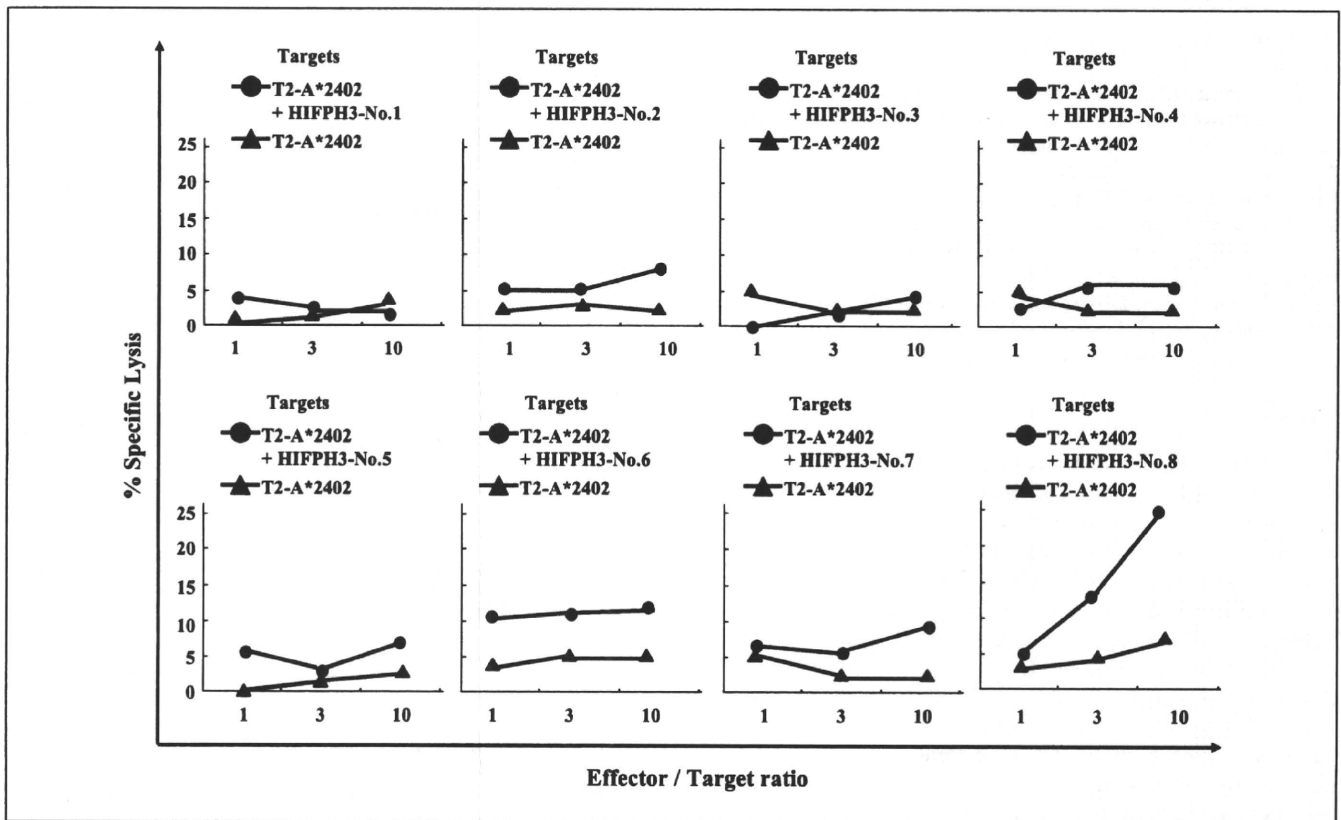
Fig. 4. Induction of HIFPH3 peptide-specific CTLs and their peptide-specific cytotoxicity. CTLs were induced from PBMCs of a HLA-A*2402$^+$ RCC patient by stimulating with group A (HIFPH3-1-HIFPH3-4) peptide-pulsed APCs (*top four graphs*) or group B (HIFPH3-5-HIFPH3-8) peptide-pulsed APCs (*bottom four graphs*). After four times of stimulation, CTLs were subjected to standard ^{51}Cr release assay at the indicated E:T ratio. Peptide-pulsed T2-A*2402 cells and nonpulsed cells were used as target cells.
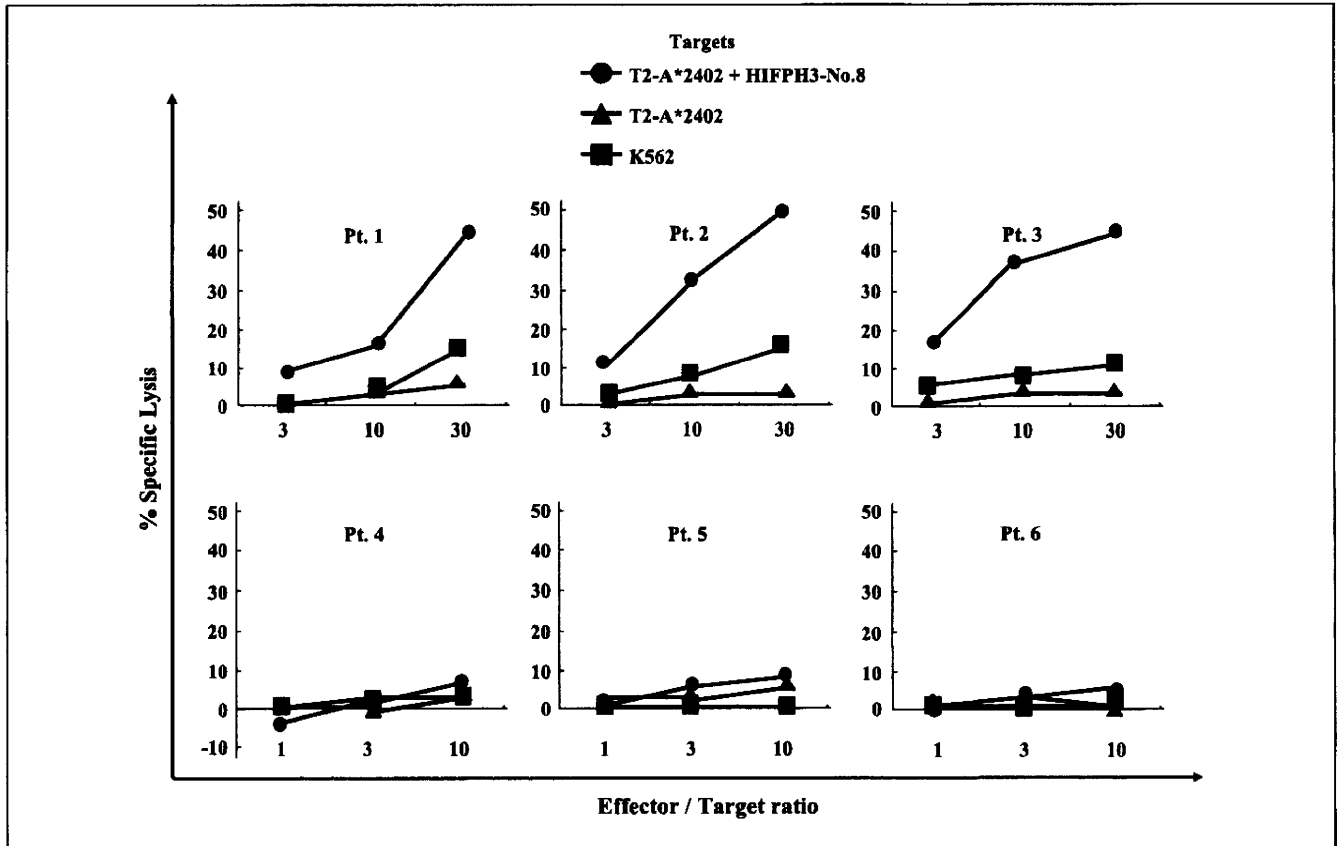
— 282 —

Fig. 5. HIFPH3-8 peptide-specific CTL induction from PBMCs of HLA-A*2402+ RCC patients. CTLs were induced from PBMCs of 6 HLA-A*2402+ RCC patients (patients 1-6) by stimulating with HIFPH3-8 peptide-pulsed APCs. The cytotoxic activity was examined by ^{51}Cr release assay at the indicated E:T ratio. HIFPH3-8 peptide-pulsed T2-A*2402 cells and nonpulsed cells were used as target cells. K562 target cells were used for monitoring natural killer activity and lymphokine-activated nonspecific cytotoxicity.

HIFPH3 positive. The histology of HIFPH3-positive cases included granular cell carcinoma, papillary RCC (Fig. 2C), and chromophobe cell carcinoma. Immunostaining of non-RCC tumors revealed that HIFPH3 was expressed in some types of tumors besides RCC, including colon cancer (Fig. 2D, 10 of 24 cases), breast cancer (Fig. 2E, 14 of 24 cases), and lung cancer (Fig. 2F, 10 of 24 cases).

Binding analysis of HIFPH3-derived peptides to HLA-A24 molecules. Because HIFPH3 is expressed in RCC cells but not in normal tissues, we hypothesized that it might be a suitable target for tumor immunotherapy. Immune tolerance toward HIFPH3 is considered to be weak because anti-HIFPH3 autoantibody was detected in sera of RCC cancer patients (data not shown). Thus, it was reasoned that antigenic peptides derived from HIFPH3 might be presented by MHC class I molecules and recognized by CD8+ T cells. To evaluate if HIFPH3 might become a target of CTLs, we focused on HLA-A*2402 allele because of its high frequency worldwide. The total amino acid sequence of HIFPH3 was searched for peptides that have HLA-A24-binding motif as 9- or 10-mer peptide with Y, F, M, or W at the second position and L, I, F, or M at the COOH-terminal position (26). Consequently, we found eight peptides (HIFPH3-1-HIFPH3-8) carrying HLA-A24-binding motif, and to assess their binding ability to HLA-A24 molecule, binding assay using T2-A*2402 cells was done as described previously (22). Two positive control peptides, HLA-A24-

restricted EBV epitope and HIV epitope, and negative control peptide, SL-8 peptide, were used in the assay. HLA-A24 level on the cell surface of T2-A*2402 cells is up-regulated in the presence of HLA-A24-binding peptides. Up-regulation of MFI of cell surface HLA-A24 was detected by flow cytometer (Fig. 3). Both EBV and HIV peptides increased MFI of HLA-A24 clearly, whereas SL-8 peptide failed, indicating adequate qualification of this assay system. HIFPH3-1 to HIFPH3-5 peptides could just increased the cell surface HLA-A24 level to mild or moderate levels, whereas HIFPH3-6 to HIFPH3-8 peptides were capable of up-regulating the HLA level to almost similar levels to EBV peptide. It was indicated that HIFPH3-6 to HIFPH3-8 might have relatively high binding affinity to HLA-A24 molecule among all the peptides.

*CTL induction from PBMCs of HLA-A*2402+ RCC patients.* To know which HIFPH3-derived peptides can be recognized by T cells of cancer patients in the context of HLA-A24, we attempted to induce peptide-specific CTL and compare their cytotoxic activity. PBMCs were collected from RCC patients with *HLA-A*2402* (patient profiles in Table 1), and T cells sorted out from the PBMCs were incubated with peptide-pulsed autologous monocyte-derived dendritic cells or autologous PHA blasts (27). Eight peptides were grouped into two peptide mixtures: group A consisting of HIFPH3-1 to HIFPH3-4, and group B consisting of HIFPH3-5 to HIFPH3-8. After four times stimulation with either of the peptide mixtures and APCs,

6921

— 283 —

cytotoxic activity against each peptide-pulsed target cells was examined by ^{51}Cr release assay. As shown in Fig. 4, CTLs induced from PBMCs by *in vitro* stimulation with group B peptides could react specifically to the HIFPH3-8-pulsed T2-A*2402 cells, whereas they could not react to HIFPH3-5, HIFPH3-6, or HIFPH3-7 peptide-pulsed target cells. The other CTLs induced by stimulation with group A peptides failed to exert cytotoxicity against HIFPH3-1, HIFPH3-2, HIFPH3-3, or HIFPH3-4 peptide-pulsed T2-A*2402 cells. Therefore, we determined that HIFPH3-8 peptide could be the best candidate for the CTL epitope presented by HLA-A*2402.

CTL induction efficiency was examined by using HIFPH3-8 peptide-pulsed autologous APCs from PBMCs of 6 RCC patients. As shown in Fig. 5, CTLs reacting specifically to HIFPH3-8 peptide-pulsed T2-A*2402 cells were successfully induced from 3 of 6 patients (patients 1-3). These data indicate that HIFPH3-8 peptide-specific CTLs could be efficiently induced from PBMCs of *HLA-A*2402*[+] RCC patients.

The results of peptide-specific CTL induction from PBMCs of RCC patients were summarized in Table 1. CTLs were not induced by pulsation with group A peptides. No. 8 peptide-specific CTLs could not be induced from two of HLA-A*2402-negative RCC patients.

Cytotoxic activity of HIFPH3-8-specific CTLs against HLA-A24[+] and HIFPH3^{+} RCC cell line. To confirm that CTLs induced with HIFPH3-8 peptide can exert cytotoxicity on HIFPH3-expressing cancer cells in the context of HLA-A*2402, we examined their cytotoxic activity against RCC cell lines: SMKT R-1 that expresses endogenous HIFPH3 and HLA-A*2402 and SMKT R-4-A*2402 that expresses both endogenous HIFPH3 and gene-transfected HLA-A*2402. As shown in Fig. 6, CTLs induced with HIFPH3-8 peptide from PBMCs of RCC patient 1 and RCC patient 3 (Table 1; Fig. 5) exerted significant cytotoxicity against SMKT R-1 and SMKT R-4-A*2402 cells but not against SMKT R-4 lacking HLA-A24 expression or K562 cells. These data implied that HIFPH3-8 peptide-specific CTLs

Fig. 6. Cytotoxic activity of HIFPH3-8-specific CTLs against HLA-A24[+] and HIFPH3^{+} RCC cell lines. CTLs were induced from PBMCs of RCC patients 1 and 3 (Table 1; Fig. 5) and their cytotoxic activity against HIFPH3^{+} HLA-A*2402[+] SMKT R-1 cells, HIFPH3^{+} HLA-A*2402[-] SMKT R-4 RCC cells, HLA-A*2402-transfected SMKT R-4-A*2402, and K562 cells was examined by ^{51}Cr release assay at the indicated E:T ratio.

were capable of recognizing endogenously processed HIFPH3-8 peptide in a HLA-A24-restricted manner.

Discussion

The process of tumor progression (proliferation, local invasion, and distant metastasis) is characterized by rapid cellular growth accompanied by alterations of the microenvironment of the tumor cells. To a large extent, the alterations in the cellular microenvironment are due to an inadequate oxygen supply and the resultant hypoxia or even anoxia (28, 29). Among these conditions, changes in the expression of genes for erythropoietin, the angiogenic vascular endothelial growth factor, transferrin receptors, and other proteins allow for the development of a more effective oxygen (and nutrient) supply. Expression of the genes for most of these proteins is regulated by HIF-1α and HIF-2α. This transcription factor was first identified by Semenza et al. as a regulator of hypoxia-induced erythropoietin expression (30-32) and has since been shown to regulate the expression of >30 target genes. These genes also play roles in tumor progression, thereby contributing to tumor aggressiveness.

The activity of the transcriptional complex of HIF is regulated by oxygen-dependent post-translational modifications that are mediated by HIFPH (HIFPH1; refs. 2, 3). HIFPHs hydroxylate two conserved proline residues of HIF-1α and HIF-2α, leading to capture by the corresponding E3 ubiquitin-ligase VHL complex and degradation (11-15). Although all three HIFPHs can hydroxylate HIF-1α and HIF-2α *in vitro*, they exhibit different patterns of expression among tissues and distinct substrate specificity (19, 33). It has been shown that HIFPH1 and HIFPH2 are expressed in various normal adult tissues and predominantly contributes to HIF-1α hydroxylation, leading to setting low steady-state levels of HIF-1α in normoxic condition (34). In contrast, as shown in our results, HIFPH3 was barely detected in normal adult tissues. It is induced in hypoxic condition and retains its activity in mediating HIF-2α hydroxylation in the condition (35), thus serving as a negative feedback loop by limiting physiologic activation of HIF in hypoxia (19, 33, 36). In the present study, we showed for the first time that HIFPH3 was overexpressed in some of RCC cell lines and tissues. Complete VHL gene sequence analysis of RCC lines revealed that 4 HIFPH3-positive RCC lines had VHL mutations and 2 HIFPH3-negative RCC lines had no mutation in VHL genes (data not shown). Therefore, it was indicated that HIFPH3 expression might be associated with VHL mutation in RCC. However, as shown in our immuno-histochemical studies, tumors without VHL mutation, such as papillary RCC and non-RCC cancers, had also expression of HIFPH3, indicating that VHL alone probably does not regulate the expression of this gene. Although we have no clear explanation about the molecular mechanism of HIFPH3 overexpression and the roles of HIFPH3 in cancer cells, its expression selectively in tumor cells indicate that it may serve as a cancer-associated antigen applicable to specific immuno-therapies. Although the frequency of HIFPH3 expression was highest among various malignant tumors that we tested, our immunohistochemical studies showed that expression of HIFPH3 was not limited to RCC. Therefore, HIFPH3 may be an immunotherapy target for lung, breast, and colon cancer besides RCC.
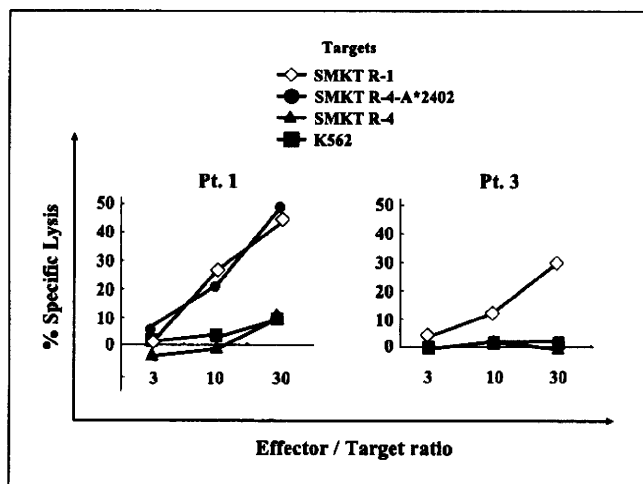
— 284 —

We identified HLA-A24-restricted CTL epitope of HIFPH3. Eight HIFPH3-derived peptides were shown to bind to HLA-A24 molecule with various affinities, and we succeeded in inducing HIFPH3-8 peptide-specific CTL from PBMCs of RCC patients. Stimulation of PBMCs from *HLA-A24*[+]/HIFPH3^{+} RCC patients with HIFPH3-8 peptide could lead to efficient induction of CTLs that exerted cytotoxicity against *HLA-A24*[+]/ HIFPH3^{+} RCC cell lines. These data indicate that HIFPH3-8 peptide might be one of the naturally processed antigenic peptides derived from HIFPH3 with considerable immunogenicity, thus serving as a potent peptide vaccine in immunotherapy for *HLA-A*2402*[+] RCC patients. In addition, we found that anti-HIFPH3 autoantibody was detectable in sera of 10 of 32 RCC patients (data not shown). These observations suggest that HIFPH3 has high antigenic potential *in vivo* in both cellular immunity and humoral immunity. Indeed, in our current study, HIFPH3-specific CTLs were successfully induced from 3 of 6 HIFPH3^{+} RCC patients' PBMCs. The reason for

CTL induction failure in 3 patients remains unknown because HIFPH3 was detected in RCC tissues by immunostaining.

In conclusion, we showed that HIFPH3 was one of potent immunogenic antigens of RCC and HIFPH3-8 peptide might serve as a tumor vaccine for HLA-A*2402[+] cancer patients. It is expected that HIFPH3 targeting immunotherapy might become a rational modality in therapy for RCC.

Disclosure of Potential Conflicts of Interest

Acknowledgments

References

1. Kattan MW, Reuter V, Motzer RJ, et al. A postoperative prognostic nomogram for renal cell carcinoma. J Urol 2001;166:63–7.
2. Robert CF, Sydney ES, Brent AB, et al. Nephrectomy followed by interferon alfa-2b compared with interferon alfa-2b alone for metastatic renal-cell cancer. N Engl J Med 2001;345:1655–9.
3. Allan JP, Arie SB, Robert AF. Nephrectomy and interleukin-2 for metastatic renal-cell carcinoma. N Engl J Med 2001;345:1711–2.
4. Boon T, Coulie PG, Van den Eynde B. Tumor antigens recognized by T cells. Immunol Today 1997;18: 267–8.
5. Rosenberg SA. A new era for cancer immunotherapy based on the genes that encode cancer antigens. Immunity 1999;10:281–7.
6. Li G, Passebose-Faure K, Lambert C, et al. Flow cytometric analysis of antigen expression in malignant and normal renal cells. Anticancer Res 2000; 20:2773–8.
7. Neumann E, Engelsberg A, Decker J, et al. Heterogeneous expression of the tumor-associated antigens RAGE-1, PRAME, glycoprotein 75 in human renal cell carcinoma: candidates for T-cell-based immunotherapies?. Cancer Res 1998;58:4090–5.
8. Hanada K, Perry-Lalley DM, Ohnmacht GA, et al. Identification of fibroblast growth factor-5 as an overexpressed antigen in multiple human adenocarcinomas. Cancer Res 2001;61:5511–6.
9. Takahashi Y, Harashima N, Kajigaya S, et al. Regression of human kidney cancer following allogeneic stem cell transplantation is associated with recognition of an HERV-E antigen by T cells. J Clin Invest 2008;118:1099–109.
10. Huang J, Zhao Q, Mooney SM, et al. Sequence determinants in hypoxia-inducible factor-1α for hydroxylation by the prolyl hydroxylases PHD1, PHD2, and PHD3. J Biol Chem 2002;277:39792–800.
11. Cockman ME, Masson N, Mole DR, et al. Hypoxia inducible factor-α binding and ubiquitylation by the von Hippel-Lindau tumor suppressor protein. J Biol Chem 2000;275:25733–41.
12. Ivan M, Kondo K, Yang H, et al. HIFα targeted for VHL-mediated destruction by proline hydroxylation: implications for O₂ sensing. Science 2001;292: 464–8.
13. Jaakkola P, Mole DR, Tian YM, et al. Targeting of HIF-α to the von Hippel-Lindau ubiquitylation complex by O₂-regulated prolyl hydroxylation. Science 2001;292:468–72.
14. Yu F, White SB, Zhao Q, et al. HIF-1α binding to VHL is regulated by stimulus-sensitive proline hydroxylation. Proc Natl Acad Sci U S A 2001;98:9630–5.
15. Bruick RK, McKnight SL. A conserved family of prolyl-4-hydroxylases that modify HIF. Science 2001;294:1337–40.
16. Ivan M, Haberberger T, Gervasi DC, et al. Biochemical purification and pharmacological inhibition of a mammalian prolyl hydroxylase acting on hypoxia-inducible factor. Proc Natl Acad Sci U S A 2002;99: 13459–64.
17. Erez N, Milyavsky M, Goldfinger N, et al. Falkor, a novel cell growth regulator isolated by a functional genetic screen. Oncogene 2002;21:6713–21.
18. Epstein AC, Gleadle JM, McNeill LA, et al. C. elegans EGL-9 and mammalian homologs define a family of dioxygenases that regulate HIF by prolyl hydroxylation. Cell 2001;107:43–54.
19. Appelhoff RJ, Tian YM, Raval RR, et al. Differential function of the prolyl hydroxylases PHD1, PHD2, and PHD3 in the regulation of hypoxia-inducible factor. J Biol Chem 2004;279:38458–65.
20. Yagihashi A, Asanuma K, Tsuji N, et al. Detection of anti-livin antibody in gastrointestinal cancer patients. Clin Chem 2003;49:1206–8.
21. Lee SP, Tierney RJ, Thomas WA, et al. Conserved CTL epitopes within EBV latent membrane protein 2: a potential target for CTL-based tumor therapy. J Immunol 1997;158:3325–34.
22. Kuzushima K, Hayashi N, Kimura H, et al. Efficient identification of HLA-A*2402-restricted cytomegalovirus-specific CD8^{+} T-cell epitopes by a computer algorithm and an enzyme-linked immunospot assay. Blood 2001;98:1872–81.
23. Sato Y, Nabeta Y, Tsukahara T, et al. Detection and induction of CTLs specific for SYT-SSX-derived peptides in HLA-A24(+) patients with synovial sarcoma. J Immunol 2002;169:1611–8.
24. Maeda A, Ohguro H, Nabeta Y, et al. Identification of human antitumor cytotoxic T lymphocytes epitopes of recoverin, a cancer-associated retinopathy antigen, possibly related with a better prognosis in a paraneoplastic syndrome. Eur J Immunol 2001;31: 563–72.
25. Sato T, Sato N, Takahashi S, et al. Specific cytotoxicity of a long-term cultured T-cell clone on human autologous mammary cancer cells. Cancer Res 1986;46:4384–9.
26. Kondo A, Sidney J, Southwood S, et al. Prominent roles of secondary anchor residues in peptide binding to HLA-A24 human class I molecules. J Immunol 1995;155:4307–12.
27. Hirohashi Y, Torigoe T, Maeda A, et al. An HLA-A24-restricted cytotoxic T lymphocyte epitope of a tumor-associated protein, survivin. Clin Cancer Res 2002;8:1731–9.
28. Vaupel P, Kallinowski F, Okunieff P. Blood flow, oxygen and nutrient supply, and metabolic microenvironment of human tumors: a review. Cancer Res 1989;49:6449–65.
29. Ryan HE, Poloni M, McNulty W, et al. Hypoxia-inducible factor-1α is a positive factor in solid tumor growth. Cancer Res 2000;60:4010–5.
30. Semenza GL, Wang GL. A nuclear factor induced by hypoxia via de novo protein synthesis binds to the human erythropoietin gene enhancer at a site required for transcriptional activation. Mol Cell Biol 1992;12:5447–54.
31. Wang GL, Jiang BH, Rue EA, et al. Hypoxia-inducible factor 1 is a basic-helix-loop-helix-PAS heterodimer regulated by cellular O₂ tension. Proc Natl Acad Sci U S A 1995;92:5510–4.
32. Wang GL, Semenza GL. Purification and characterization of hypoxia-inducible factor 1. J Biol Chem 1995;270:1230–7.
33. Cioffi CL, Liu XQ, Kosinski PA, et al. Differential regulation of HIF-1α prolyl-4-hydroxylase genes by hypoxia in human cardiovascular cells. Biochem Biophys Res Commun 2003;303:947–53.
34. Berra E, Benizri E, Ginouves A, et al. HIF prolyl-hydroxylase 2 is the key oxygen sensor setting low steady-state levels of HIF-1α in normoxia. EMBO J 2003;22:4082–90.
35. Nakayama K, Frew IJ, Hagensen M, et al. Siah2 regulates stability of prolyl-hydroxylases, controls HIF1α abundance, and modulates physiological responses to hypoxia. Cell 2004;117:941–52.
36. Hirsila M, Koivunen P, Gunzler V, et al. Characterization of the human prolyl 4-hydroxylases that modify the hypoxia-inducible factor. J Biol Chem 2003; 278:30772–80.

— 285 —

Downregulation of *Tie2* gene by a novel antitumor sulfolipid, 3'-sulfoquinovosyl-1'-monoacylglycerol, targeting angiogenesis

Yoko Mori,[1] Hiroeki Sahara,[1,5] Kayo Matsumoto,[1] Nobuaki Takahashi,[1] Takayuki Yamazaki,[3] Keisuke Ohta,[3] Satoko Aoki,[3] Masahiko Miura,[4] Fumio Sugawara,[3] Kengo Sakaguchi[3] and Noriyuki Sato[2]

[1]Marine Biomedical Institute, [2]Department of Pathology, Sapporo Medical University School of Medicine, S1, W17, Chuo-ku, Sapporo 060-8556; [3]Department of Applied Biological Science, Frontier Research Center for Genomic Drug Discovery, Tokyo University of Science, 2641 Yamazaki, Noda, Chiba 278-8510; [4]Oral Radiation Oncology, Department of Oral Restitution, Graduate School, Tokyo Medical and Dental University, Yushima, Bunkyo-ku, Tokyo, Japan

We previously reported that 3'-sulfoquinovosyl-1'-monoacylglycerol (SQMG) was effective in suppressing the growth of solid tumors due to hemorrhagic necrosis *in vivo*. In the present study, we investigated the antiangiogenic effect of SQMG. *In vivo* assessment of antitumor assays showed that some tumor cell lines, but not others, were sensitive to SQMG. Microscopic study suggested that in SQMG-sensitive tumors, but not SQMG-resistant tumors, angiogenesis was reduced. We next investigated gene expression relating to angiogenesis in tumor tissues by quantitative real-time polymerase chain reaction. Consequently, although vascular endothelial growth factor gene expression was not detected with significant differences among the cases, significant downregulation of *Tie2* gene expression was observed in all SQMG-sensitive tumors as compared with controls, but not in SQMG-resistant tumors. These data suggested that the antitumor effects of SQMG could be attributed to antiangiogenic effects, possibly via the downregulation of *Tie2* gene expression in SQMG-sensitive tumors. (*Cancer Sci* 2008; 99: 1063–1070)

A ngiogenesis, the formation of new blood vessels, is a fundamental process required for normal embryonic development and for the development of pathological conditions such as cancer.[1,2] Its importance in solid tumor growth and metastasis has been widely recognized by multiple studies.[2] Therefore, antiangiogenic treatments may be a promising target for the treatment of cancer. For example, it was reported that agents such as angiostatin, endostatin, and anti-vascular endothelial growth factor (VEGF) antibodies that inhibited VEGF receptor tyrosine kinase were developed, resulting in effective inhibition of solid tumor growth *in vivo*.[3–9] However, it was reported that the receptor tyrosine kinase Tie2 could play a critical role in tumor-induced angiogenesis.[10,11] It was also demonstrated that the suppression of Tie2 signaling caused by using specific blocking agents such as soluble dominant-negative receptors,[11–14] an antisense oligonucleotide,[15] RNA aptamers and RNA interference,[16,17] and a short synthetic peptide[18] resulted in antitumor effects by influencing anti-angiogenesis. Thus, therapeutic antiangiogenesis for cancer treatment using multiple strategies was reported and its importance has been widely recognized as a promising treatment for cancer chemotherapy. However, there are few reports about chemotherapeutic compounds for cancer targeting Tie2.

We previously reported that the growth of human adenocarcinoma tumors treated with 3'-sulfoquinovosyl-1'-monoacylglycerol (SQMG) was inhibited, and these tumors showed extensive hemorrhagic necrosis by pathohistological examination.[19,20] However the mechanism by which hemorrhagic necrosis occurs via the antiangiogenesis activity of SQMG remains undefined. Recently, Sakimoto *et al.* reported that combined treatment with

α-SQMG (C18:0) and radiation synergistically inhibited the growth of human tumors transplanted into nude mice, accompanied by a significant reduction in the vascularity of the tumors.[21] Here, we demonstrate that the antitumor effects of SQMG could be attributed to inhibition of tumor antiangiogenesis, which seems to be involved in downregulation of the *Tie2* gene. Thus, SQMG is a promising candidate as an antitumor drug targeting angiogenesis.

Materials and Methods

Synthesis of SQMG. The chemical structure of the synthesized compound SQMG containing fatty acid 18:1 (oleic acid C18:1) is shown in Figure 1. The procedure for synthesis of SQMG was described previously.[20]

Cell lines. Human breast adenocarcinoma MDA-MB-231, lung adenocarcinoma A549, colon adenocarcinoma WiDr, prostate adenocarcinoma PC-3, tongue squamous cell carcinoma SAS, esophagus squamous cell carcinoma TE-8, lung small cell carcinoma LU65 lines, and mouse normal fibroblast NIH3T3 were used in the present study. MDA-MB-231, A-549, WiDr, PC-3, and NIH3T3 were provided by the Japanese Cancer Research Resources Bank. SAS, Lu65, and TE-8 cells were obtained from Health Science Research Resources Bank (Sendai, Japan). A549, WiDr, PC-3, SAS, TE-8, and Lu65 cells were cultured with RPMI1640 supplemented with 10% fetal calf serum, 200 U/mL penicillin, 200 μg/mL streptomycin, and 2 mM L-glutamine. MDA-MB-231 was cultured with Leibovitz's L15 supplemented with 10% fetal calf serum, 200 U/mL penicillin, 200 μg/mL streptomycin, and 2 mM L-glutamine. Human umbilical vein endothelial cells (HUVEC) were purchased from Cambrex (Walkerville, MD, USA) and maintained according to the provider's instructions. Cells in passage numbers three to five were used for this study.

***In vivo* assessment of antitumor assay.** Inbred mice, female BALB/c nu/nμ mice (20–22 g, 7 weeks of age) were obtained from Japan SLC (Shizuoka, Japan). All procedures were carried out in compliance with the guidelines of the Animal Research Center of Sapporo Medical University. Human tumor cells from lines MDA-MB-231, A549, WiDr, PC-3, SAS, TE-8, and LU65 (10^6 cells/mouse) suspended in phosphate-buffered saline (PBS) were injected subcutaneously into a dorsal side of the mice. After implantation, the tumor sizes in all of these mice were measured at 2-day intervals. When the solid tumors grew to 30–40 mm³ in tumor volume (tumor volume = length × [width]²

5To whom correspondence should be addressed.
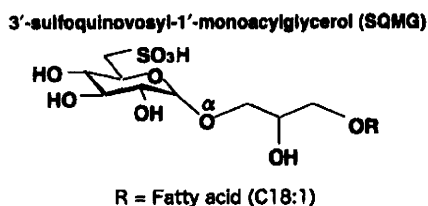E-mail: hsahara@sapmed.ac.jp.

Fig. 1. Structure of 3'-sulfoquinovosyl-1'-monoacylglycerol (SQMG). SQMG contains a single fatty acid, R = C18:1.

× 0.5), SQMG was administrated every day for 14 days, and the tumor growth was observed. Each type of tumor was divided randomly into two or three groups ($n = 4$/group). A control group was injected intraperitoneally with 0.2 mL saline solution, and test groups were injected intraperitoneally with SQMG at a dose of 5 or 20 mg/kg every day for 14 days. On the next day after the last administration of SQMG, the tumor size was measured, and tumors were excised and prepared for further study. The mean ± SE tumor volume from each group ($n = 4$/group) is shown (Fig. 2). The growth of each tumor was analyzed using Student's t-test.

Immunohistochemical study. All tumors excised from mice ($n = 4$/group) were embedded in Tissue-Tek OCT Compound (Sakura Finetek USA, Torrance, CA, USA) and frozen. Acetone-fixed cryosections were stained with an antimouse CD31 mono-clonal antibody, and then antirat IgG conjugated with AlexaFlour 488 (BD Bioscience Pharmingen, CA, USA) as a secondary antibody. Nuclei were counterstained with propidium iodide (PI) (Vector Laboratories, Burlingame, CA, USA). The CD31-positive ring-form blood vessels in 500-mm²-section areas of these samples were counted at ×100 magnification under a fluorescence microscope (Olympus AX80; Olympus, Tokyo, Japan) and is represented as the mean ± SE of four section areas from each group. The results were analyzed using Student's t-test.

3-(4,5-Dimethylthiazol-2-yl)-2,5-diphenylthtrazolium bromide assay and annexin V labeling assay. To investigate the cytotoxicity of SQMG, the 3-(4,5-dimethylthiazol-2-yl]-2,5-diphenylthtrazolium bromide (MTT) assay was carried out using HUVEC and NIH3T3 cells according to methods described previously.[19,20] Briefly, cells (5×10^3 cells/well) were cultured in 96-well plates for 24 h and then various amounts of SQMG suspended in PBS were added to the wells. Following cultivation for 48 h, 50 µg MTT was added to cells and incubation was continued for 3 h. Then 4% HCl in 2-propanol was added to each well and mixed by pipette to disrupt the cells. The absorbance of each well was measured using a multiwell scanning photometer (Micro ELISA MR600; Dynatech Laboratories, Alexandria, VA, USA) at a wavelength of 570 nm. Results were represented as the mean ± SE of triplicate wells in one of three independent experiments. The annexin V labeling assay was carried out for detection of apoptotic HUVEC. HUVEC (10^6 cells) cultured in six-well plates for 48 h in the presence or absence of various amounts of SQMG were suspended in PBS. Following cultivation, cells were double-stained with annexin-V–fluorescein and PI using the Annexin-V-FLUOS staining kit according to the manufacturer's instructions (Roche Applied Science, Penzberg, Germany). The percentage of apoptotic (annexin V and PI double positive) cells was determined by flow cytometric analysis (FACS Calibur and Cell Quest software; BD Bioscience). The results are represented as the mean ± SE of three independent experiments.

Angiogenesis assay. The angiogenesis assay was done using an Angiogenesis Kit (Kurabo, Osaka, Japan) according to the manufacturer's instructions. Briefly, HUVEC grown on human diploid fibroblast sheets on Matrigel (Kurabo, Osaka, Japan) were cultured with or without SQMG at the indicated concentrations

in growth medium containing 10 ng/mL VEGF-A for 14 days. Fresh growth medium with or without SQMG was replaced 4, 7, and 9 days after incubation. After incubation, cells were fixed in 70% ethanol and immunostained with an anti-CD31 antibody for 1 h and detected using the alkaline phosphate method. The tube-formation areas of HUVEC were quantitated using Image ++ software downloaded from the internet (http://www.pluto.dti.ne.jp/~horie-ms/index-j.html). The results are represented as the mean ± SE of five independent areas. In some experiment, HUVEC grown on human diploid fibroblast sheets on Matrigel were cultured for 14 days, and then in the presence or absence SQMG for 2 days. Subsequently, the cell-derived total RNA was harvested and quantitated for the amount of mRNA copy of human VEGF receptor-1 (Flt-1), VEGF receptor-2 (KDR), and Tie2 by quantitative real-time reverse transcription (RT)–polymerase chain reaction analysis (PCR).

Quantitative real-time RT-PCR analysis. Tumor-derived total RNA was prepared using an RNeasy Mini Kit (Qiagen, Hilden, Germany) according to the manufacturer's instructions and then reverse transcribed to cDNA with a Transcriptor First Strand cDNA Synthesis Kit (Roche Applied Science). Measurement of gene expression by quantitative analysis was carried out using a LightCycler system (Roche Applied Science). Primers and hybridization probes were synthesized by Nihon Gene Research Laboratory (Sendai, Japan). Quantitative real-time RT-PCR analysis of human $VEGF_{165}$, mouse angiopoitin-1 (*Ang1*), mouse angiopoitin-2 (*Ang2*), human *Flt-1*, human *KDR*, human *Tie2*, human *CD31*, and human glucose-6-phosphate dehydrogenase (*G6PDH*) gene expression was carried out using a LightCycler FastStart DNA Master[PLUS] SYBR Green I system (Roche Applied Science) with primer sets described in Table 1. Detection of gene expression of mouse *Flt-1*, VEGF receptor-2 (*Flk-1*), *Tie1*, *Tie2*, *CD31*, *SM22α*, and *G6PDH* was carried out using a LightCycler FastStart DNA Master HybProbe system (Roche Applied Science) with primer sets and probes described in Table 1. PCR amplification of the housekeeping gene *G6PDH* was carried out for each sample as a control for sample loading and to allow normalization among samples. To determine the absolute copy number of the target transcripts, the amplified fragments of *G6PDH* or target genes amplified by PCR using the above-described primer sets were constructed using the pCR4-TOPO cloning vector (Invitrogen, Carlsbad, CA, USA), and the concentrations of these purified plasmids were measured. The absorbance at 260 nm and copy numbers were calculated from the concentrations of samples. A standard curve was created by plotting the threshold cycle versus the known copy number for each plasmid template in the dilutions. The copy numbers for all unknown samples were determined according to the standard curve using LightCycler software 3.5.3 (Roche Applied Science). To correct differences in both RNA quality and quantity between samples, each target gene was first normalized by dividing the copy number of the target by the copy number of *G6PDH* (copy number of target/copy number of *G6PDH* = normalized target gene). The initial value of *G6PDH* corrected for the amount of *G6PDH* was indicated as 100% to evaluate the sequential alteration of the mRNA expression level. For mouse genes, each sample was corrected with the copy number of the murine *CD31* or *SM22α* gene as markers for endothelial cells and pericytes, respectively.[22,23] Thus, this represents the amount of target gene expression in an endothelial cell or pericyte, not in a human tumor cell. Results were represented as the mean ± SE of four RNA samples from each group ($n = 4$/group), and analyzed using Student's t-test.

Results

In vivo assessment of antitumor effects of SQMG. Seven human tumor cell lines, MDA-MB-231, A549, WiDr, PC-3, SAS,

Table 1. Primer and probe for quantitative real-time reverse transcription–polymerase chain reaction

Gene	Forward primer (5'-3')	Reverse primer (5'-3')	5' LCRed640 probe (5'-3')	3' Fluorescein probe (5'-3')
Mouse Flt-1	GGCTTTGCAGATCCACAT	GCAGAGTGCTAGTGTCCAG	TCCAGGCTCATGAATTTGAAAGCGTTTACAT	TCGGTGAAAGCTCCTCAAAGGTTTTGATTCT
Mouse Flk-1	AAGCGGGACGAGGAGAGA	CCCATGTGGACCGATGTT	AAGCTTGTACCACGTGAGGTTCTCAAACG	ATTTCTGTCTGCAGTGCACAACAGGGACA
Mouse Tie1	GAAGGAGGAGAAGGAGGCT	CAGGAAACCATCACCGGA	CAGCAAAGGCTCAGGACAGTCAGTAGTCAT	ACGTGCCAGCTCTCTAGCCAGGGCT
Mouse Tie2	CGGACTGACTACGAGCTGT	GTTGTTGCAGGGATCGC	CTCTTGGAGGAGGAGTCCGATAGACG	TGTTGTAAATCGTCTCACAGGCCCAGGA
Mouse CD31	CACCTATGAAAGCAAAGAG	AATCACAACTCATCCACTG	TGTTGCTGGGTCATTGGAGGTCACCT	TTCCATGTCTCTGGTGGGGCTTATCTGTGA
Mouse SM22α	GGAGATCCCAACTGGTTATG	AGAGCTGTCAGG GCTAAGAAC	GAGGGAAGCACGTCATTGGCCTT	AGAGGGACTTCACAGACAGCCAACTGCA
Mouse G6PDH	GCACAAGATTGATCGAGA	GAGGCAGAGTATAGATGGTGTA	CTTGTAGGTACCCTCGTACTGGAAGCCCA	TCTCTTCATCAGCTCATCTGCCTCTGTGG
Mouse Ang1	GCATCTGGAGCATGTGATG	TAGCAGTTGTATTTCAAGTCG		
Mouse Ang2	GAAGAGCGTGGACAGCACAGG	GAGTCGTCGTAGTCGAGGGG		
Human VEGF₁₆₅	AGAGCAAGACAAGAAAATCC	TACAAACAAATGCTTTCTCC		
Human Flt-1	GACTGACAGCAAACCCAAG	AGCGTGGTCGTAGGTGAAC		
Human KDR	TGGTCTCTCGGTTGTGTATG	AAGGGTATGGGTTTGTCACTG		
Human Tie2	CAAACCCGTTAATCACTATG	TCCGATAGAAGCGTTGTGTG		
Human CD31	CAACTTTAAAAACAAGTAA	AATCTGGACCTCATCCACCG		
Human G6PDH	CTGCGTTATCCTCACCTTC	CGGACGTCATCTGAGTTG		

TE-8, and LU65, were injected subcutaneously into mice, and then these mice bearing solid tumors that grew to 30–40 mm³ in tumor volume were injected intraperitoneally with saline or SQMG every day for 14 days. As shown in Figure 2, SQMG treatment of mice bearing MDA-MB-231, A549, WiDr, and SAS solid tumors, injected with 5 and 20 mg/kg SQMG showed significant inhibition of tumor growth as compared with the control group on the next day after the last injection date. None of the mice showed any significant loss of bodyweight throughout the experiment period (data not shown). In contrast, mice bearing PC-3, TE-8, and LU65 solid tumors injected with SQMG did not show tumor growth inhibition as compared with the control on the day after the last injection. These data demonstrate that four tumor lines, MDA-MB-231, A549, WiDr, and SAS, were sensitive to SQMG (SQMG-sensitive), but three lines, PC-3, TE-8, and LU65 were resistant (SQMG-resistant).

Antiangiogenesis activity of SQMG in vivo. We previously indicated that SQMG treatment results in hemorrhagic necrosis in tumors. To investigate the mechanism of the antitumor effects of SQMG, we first carried out immunohistochemical analysis to determine the angiogenesis profiles in tumors. Tumors were excised from mice on the next day after the last injection and cryosections of these acetone-fixed tumors were stained with antimouse CD31 monoclonal antibody as an endothelial cell marker. Representative photos showing immunohistochemical staining of MDA-MB-231 tumors treated with or without SQMG are presented in Figure 3, in which CD31-positive ring-form blood vessels are clearly observed for both the control (Fig. 3a,b) and SQMG treatment (Fig. 3c,d). Therefore, the CD31-positive ring-form blood vessels of all samples in 500-mm²-section areas were counted under a fluorescence microscope. Consequently, as shown in Table 2, in all four SQMG-sensitive tumors treated with 20 mg/kg SQMG, the numbers of blood vessels were significantly decreased ($P < 0.01$) with SQMG treatments, as compared with controls. In contrast, in all three of the SQMG-resistant tumors treated with 20 mg/kg SQMG, there were no significant differences in the number of blood vessels between controls and SQMG treatments. These data suggested that the antitumor effect of SQMG could be attributed to the inhibition of tumor angiogenesis.

Inhibitory effect of SQMG on endothelial cell-derived capillary formation in vitro. To investigate whether SQMG directly affected the growth profile of endothelial cells, we assessed proliferation and cytotoxicity by using the human endothelial cell line HUVEC. SQMG was added to HUVEC in concentrations from 0 to 100 μM, and cell proliferation and apoptosis were analyzed using the MTT assay and annexin V labeling assay, respectively. As shown in Figure 4a, there was no obvious the inhibitory effect on the proliferation of HUVEC up to the concentration of 25 μM. When 50 or 100 μM SQMG was added to cells, the cell proliferation was inhibited to 71.5 ± 5.6 or 55.3 ± 4.5%, respectively. Meanwhile, when SQMG at concentrations from 0 to 50 μM was added to cells, 8.5–13.3% of cells were observed to be apoptotic. However, when 100 μM SQMG was added to cells, apoptotic effects were increased to 33.8 ± 11.6%, suggesting that there was minimal weak influence on the apoptosis of HUVEC up to the concentration of 50 μM SQMG (Fig. 4b).

We further considered that it would be important to evaluate the antiangiogenic activity of SQMG using an angiogenesis model in vitro that is considered to closely represent in vivo situations. It is well known that HUVEC cocultured with fibroblast cells on Matrigel form capillary networks with tube-like structures and adopt characteristics of newly formed blood vessels.[21] Before investigating the influence of SQMG on the formation of these structures, we studied fibroblast cell proliferation and cytotoxicity using mouse NIH3T3 instead of human normal fibroblasts by MTT assay. Consequently, there was no obvious
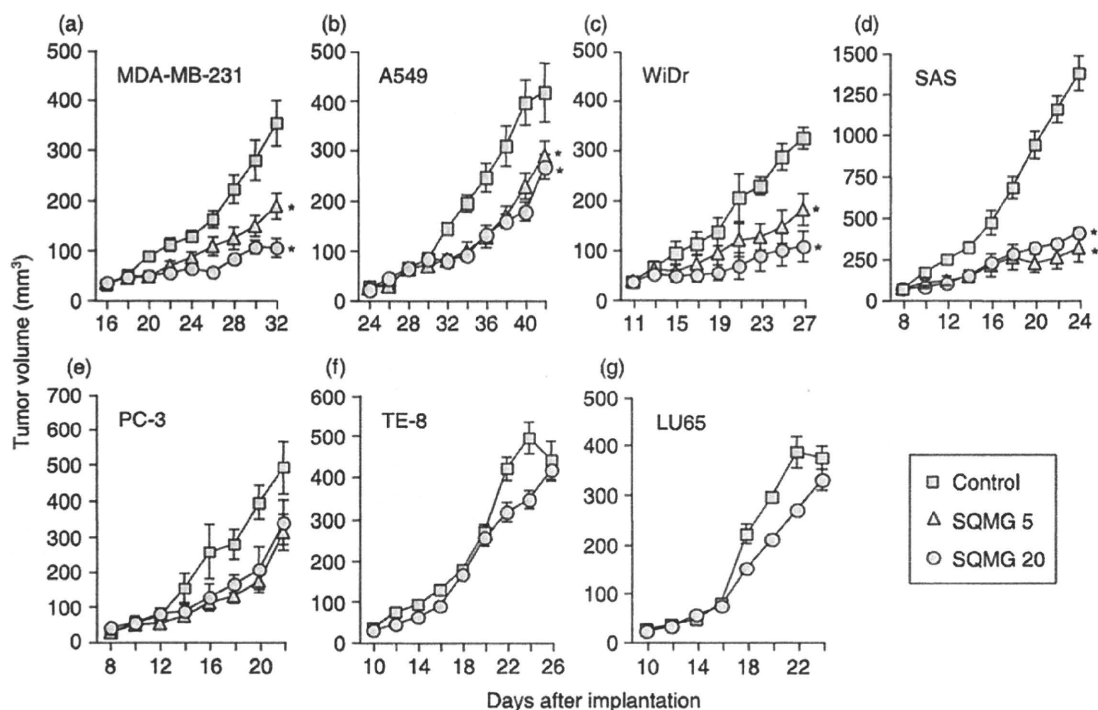
Mori et al.

– 288 –

Fig. 2. *In vivo* study of the antitumor effects of 3′-sulfoquinovosyl-1′-monoacylglycerol (SQMG). Human tumor cells (10^6) of the cell lines (a) MDA-MB-231, (b) A549, (c) WiDr, (d) SAS, (e) PC-3, (f) TE-8, and (g) LU65 were injected subcutaneously into mice, and when tumors grew to 30–40 mm³, mice were injected with saline (control), 5 mg/kg (SQMG 5), or 20 mg/kg (SQMG 20) every day for 14 days. The means ± SE of tumor volumes from each group (n = 4/group) are shown. *$P < 0.01$.
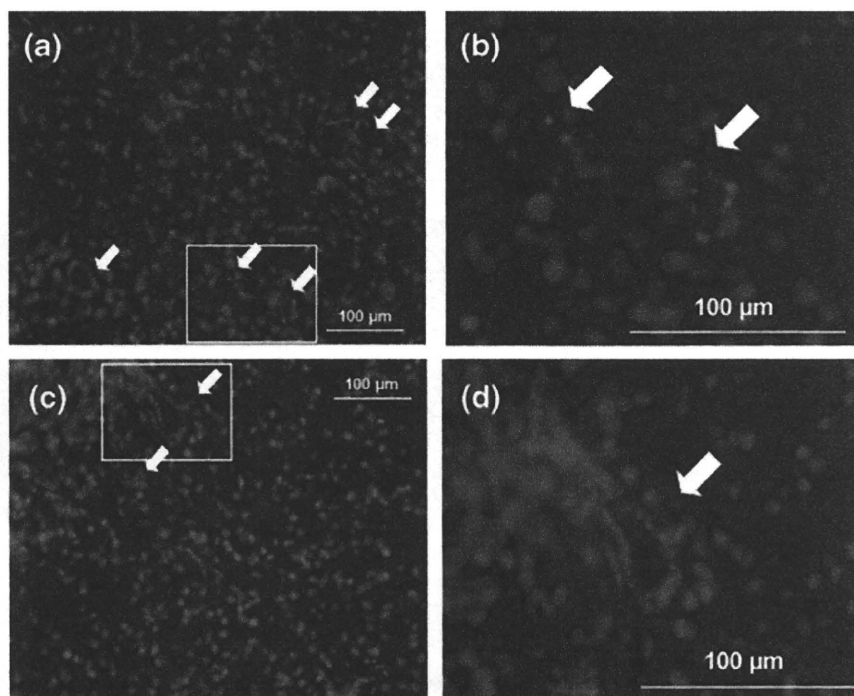

Fig. 3. Antiangiogenesis assessment by immunohistochemical analysis. Cryosections of MDA-MB-231 treated (a,b) without and (c,d) with 3′-sulfoquinovosyl-1′-monoacylglycerol were stained with antimouse CD31 monoclonal antibody and antirat IgG conjugated with AlexaFlour 488, and nuclei were counterstained with propidium iodide. Arrows indicate CD31-positive blood vessels. Insets in (a) and (c) are magnified and shown in (b) and (d), respectively. Scale bar = 100 μm.

cytotoxic potential up to the concentration of 100 μM SQMG (Fig. 4c). Meanwhile, when 50 μM SQMG was added to these cells, capillary network formation was markedly inhibited compared with the control (Fig. 5a–c). Quantitation of these capillary areas by Image ++ software showed that the capillary formation treated with 50 μM SQMG was reduced approximately

70% compared with the control (Fig. 5d). Thus, these data suggest that SQMG could influence capillary formation.

Influence of SQMG on *VEGF* gene expression in tumor tissues. It is known that angiogenesis is basically dependent on VEGF.[1,2] We next quantified the mRNA copy number of tumor-derived $VEGF_{165}$ in mice bearing tumors treated with or without 5 and

Table 2. Number of tumor-induced blood vessels in tumor tissues

Criteria	Tumor	No. blood vessels (500 mm²)	
		Control	SQMG
	MDA-MB-231[†]	10.2 ± 1.0	2.3 ± 1.8*
	A549	6.3 ± 1.1	2.9 ± 0.3*
Sensitive	WiDr	13.4 ± 4.2	6.6 ± 2.6*
	SAS	15.2 ± 1.3	7.2 ± 1.6*
	PC-3	10.7 ± 1.7	11.9 ± 2.7
Resistant	TE-8	11.4 ± 2.4	11.7 ± 1.9
	LU65	6.2 ± 2.2	3.8 ± 1.1

[†]Data are presented as mean ± SE. *$P < 0.01$. SQMG, 3'-sulfoquinovosyl-1'-monoacylglycerol.

20 mg/kg SQMG by quantitative real-time RT-PCR. *G6PDH* expression was used as a housekeeping gene control. Consequently, as indicated in Table 3, in all four SQMG-sensitive and the three resistant models, the mRNA copy number of human $VEGF_{165}$ did not show any overt difference between controls and SQMG treatment groups, suggesting that SQMG did not influence *VEGF* gene expression. In our preliminary experiments using enzyme-linked immunosorbent assay, VEGF secretion in SQMG-sensitive MDA-MB-231 and SQMG-resistant TE-8 tumor tissues did not differ between controls and SQMG treatment groups (data not shown).

Influence of SQMG on angiopoietin expression in tumor tissues. We next quantified the mRNA copy numbers of *Ang1* and *Ang2*, which are known as important factors for vascular remodeling. Because Ang1 and Ang2 are expressed mainly in pericytes and endothelial cells, respectively,[10] the amounts of their expression in mice were adjusted with the amounts of *G6PDH*-normalized $SM22\alpha$ and *CD31*, respectively ([mRNA copy number of target gene/mRNA copy number of G6PDH]/[mRNA copy number of SM22α or CD31/mRNA copy number of G6PDH]).[23] In the SQMG-sensitive tumors MDA-MB-231, A549, and SAS, the mRNA copy numbers of *Ang1* in SQMG-treated tumors appeared to have a tendency to increase two- to three-fold (Table 4), whereas this was not true for *Ang2*.

Downregulation of *Tie2* gene expression in SQMG-sensitive tumors. We demonstrated that although SQMG had less effect on cytotoxic activity against endothelial cells *in vitro* and on VEGF secretion *in vivo*, it strongly inhibited angiogenesis *in vitro* and *in vivo*. To investigate the reasons why the number of mouse-derived blood vessels was decreased by SQMG treatment, we next quantified the mRNA copy numbers of receptor genes related to angiogenesis that are expressed on the endothelial cell surface, namely, *Flt-1*, *Flk-1*, *Tie1*, and *Tie2*, by quantitative real-time RT-PCR. The expression profiles of these genes were calculated with the following formula using the mRNA copy number of each gene, as shown previously:[23]

$$(\text{target gene/G6PDH})/(\text{CD31/G6PDH}).$$

Fig. 4. Influence of 3'-sulfoquinovosyl-1'-monoacylglycerol (SQMG) on cell proliferation and apoptosis. (a) Human umbilical vein endothelial cells (HUVEC) and (c) NIH3T3 were cultured in the presence or absence of SQMG at the indicated concentrations. Cell proliferation was examined by MTT assay. Results represent means ± SE of triplicate wells on one of three independent experiments. (b) HUVEC were cultured in the presence or absence of SQMG at the concentrations indicated for 48 h, harvested, and double-stained with annexin-V–fluorescein and propidium iodide (PI). The percentage of apoptotic (annexin V and PI double positive) cells was determined by flow cytometric analysis. Results represent means ± SE of three independent experiments.
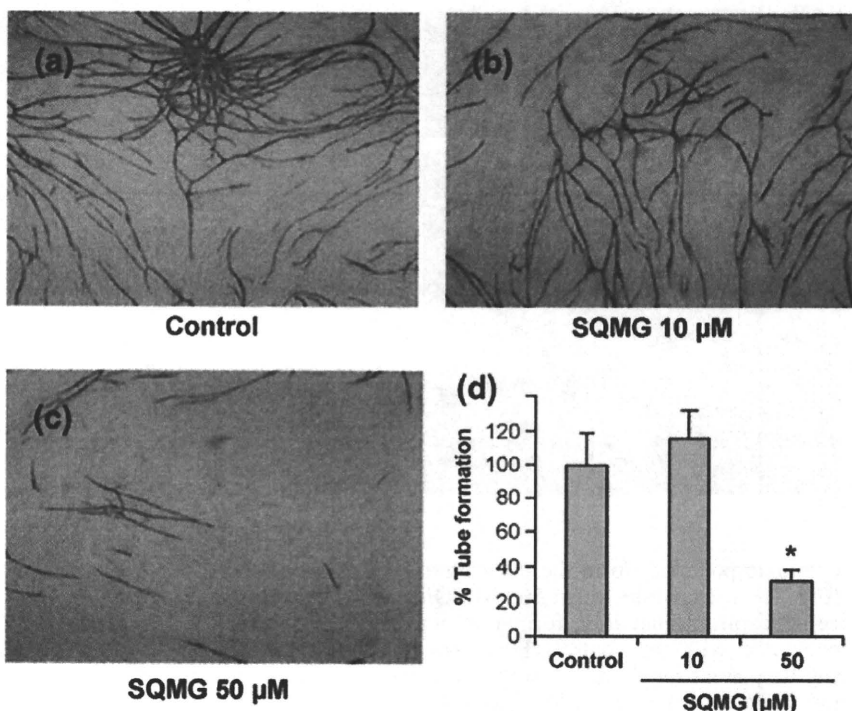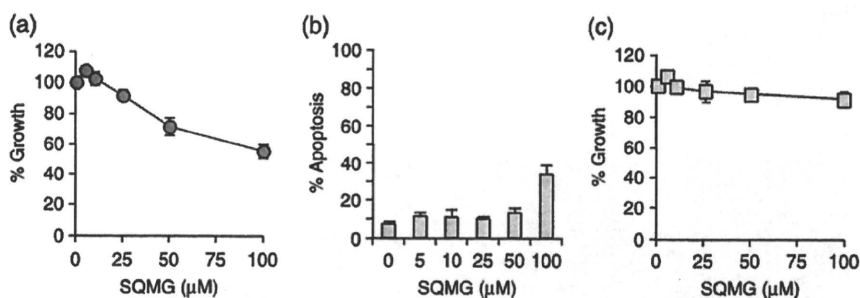

Fig. 5. Effect of 3'-sulfoquinovosyl-1'-monoacylglycerol (SQMG) on angiogenesis *in vitro*. (a–c) Human umbilical vein endothelial cells (HUVEC) grown on a fibroblast sheet on Matrigel were cultured (a) without and (b,c) with SQMG at the indicated concentrations. After cultivation, the cells were fixed and stained with an antihuman CD31 antibody for 1 h. CD31 molecules were detected using the alkaline phosphate method. (d) The tube formation of HUVEC was quantitated using Image ++ software. Results represent means ± SE of five independent areas on one of three independent experiments. *$P < 0.01$.

Mori *et al.*

Table 3. Human vascular endothelial growth factor (*VEGF*) gene expression in tumor tissues treated without or with 3′-sulfoquinovosyl-1′-monoacylglycerol (SQMG)

Criteria	Tumor	mRNA copy number (human $VEGF_{165}$/G6PDH)		
		Control	SQMG-5[‡]	SQMG-20[‡]
Sensitive	MDA-MB-231[†]	2.71 ± 0.63	2.76 ± 0.61	2.91 ± 0.81
	A549	0.15 ± 0.01	0.21 ± 0.06	0.18 ± 0.03
	WiDr	4.43 ± 0.61	2.40 ± 0.05	2.37 ± 0.42
	SAS	1.89 ± 0.14	1.99 ± 0.04	1.67 ± 0.1
	PC-3	0.58 ± 0.11	0.63 ± 0.04	0.66 ± 0.01
Resistance	TE-8	1.54 ± 0.56	ND	1.76 ± 0.58
	LU65	3.23 ± 0.43	ND	3.25 ± 0.82

[†]Data are presented as mean ± SE. G6PDH, glyceraldehyde-6-phosphate dehydrogenase; ND, not done; SQMG 5, treatment with 5 mg/kg SQMG; SQMG 20, treatment of 20 mg/kg SQMG.

As shown in Table 5, the mRNA copy number of the mouse *Flt-1* gene per copy of the *CD31* gene, which is expressed on mouse endothelial cells in tumor tissues, was similar in controls and after SQMG treatment. This was also true for the mRNA copy number of mouse *Flk-1* in most tumor tissues other than SAS tumors. Only in A549 did *Tie1* gene expression seem to be influenced by SQMG treatment. In contrast, the mRNA copy number of mouse Tie2 in tumor tissues was significantly down-regulated in all SQMG-sensitive tumors but not in SQMG-resistant tumors, suggesting that SQMG might affect mouse *Tie2* gene expression in the endothelial cells.

We further investigated whether *Flt-1*, *KDR*, and *Tie2* gene expression in capillary-formed HUVEC were influenced by SQMG *in vitro*. As shown in Figure 6, although *Flt-1* and *KDR* expression were not influenced, *Tie2* gene expression in capillary-formed HUVEC was also downregulated to approximately 50% lower than the control level when 50 μM SQMG was added to cells. Taken together, the data suggest that SQMG plays a role in downregulating *Tie2* gene expression *in vivo* and *in vitro*.

Table 4. Mouse angiopoietin (Ang) gene expression in tumor tissues

Tumor	Treatment	mRNA copy number ratio	
		Ang-1/SM22α	Ang-2/CD31
MDA-MB-231	Control	0.045 ± 0.015	0.158 ± 0.053
	SQMG 5	0.187 ± 0.095*	0.312 ± 0.078
	SQMG 20	0.120 ± 0.047*	0.300 ± 0.103
A549	Control	0.028 ± 0.003	1.838 ± 1.087
	SQMG 5	0.041 ± 0.008*	1.422 ± 0.746
	SQMG 20	0.054 ± 0.028*	4.346 ± 5.406
WiDr	Control	0.021 ± 0.001	0.400 ± 0.021
	SQMG 5	0.017 ± 0.002	0.409 ± 0.053
	SQMG 20	0.022 ± 0.005	0.458 ± 0.059
SAS	Control	0.035 ± 0.025	0.355 ± 0.167
	SQMG 5	0.093 ± 0.047*	0.390 ± 0.185
	SQMG 20	0.091 ± 0.051*	0.448 ± 0.109
TE-8	Control	0.008 ± 0.001	0.228 ± 0.067
	SQMG 5	ND	ND
	SQMG 20	0.009 ± 0.001	0.182 ± 0.100
LU65	Control	0.008 ± 0.001	0.237 ± 0.184
	SQMG 5	ND	ND
	SQMG 20	0.011 ± 0.001	0.225 ± 0.046
PC-3	Control	0.572 ± 0.212	0.295 ± 0.054
	SQMG 5	0.172 ± 0.024	0.340 ± 0.176
	SQMG 20	0.301 ± 0.077	0.392 ± 0.040

*P-values are in the range of 0.22–0.54.
Data are presented as mean ± SE. ND, not done; SQMG 5, treatment of 5 mg/kg SQMG; SQMG 20, treatment of 20 mg/kg SQMG.

Discussion

In the present study, we demonstrated that SQMG induced anti-angiogenic effects in tumor xenografts, resulting in inhibition of solid tumor growth. As significant decreases in tumor angiogenesis were observed in SQMG-sensitive tumors but not in SQMG-resistant tumors, it was speculated that the antitumor
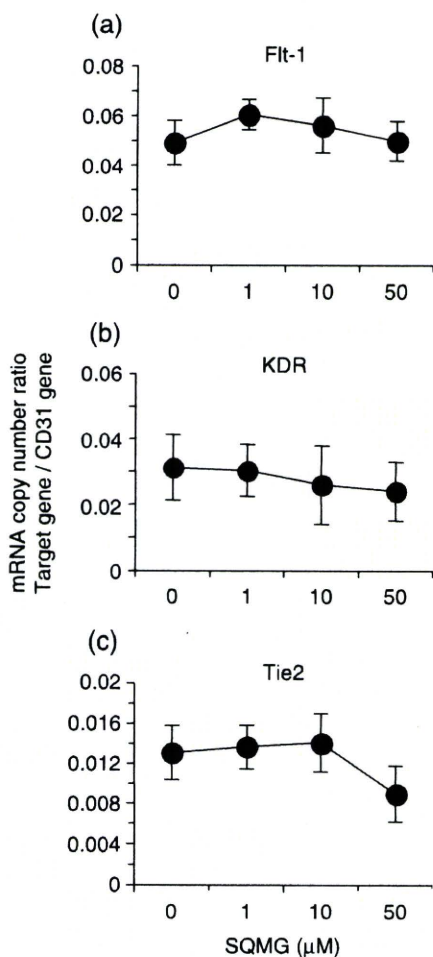
Table 5. Angiogenic receptor gene expression on mouse endothelial cells in tumors

Tumor	Treatment	mRNA copy number ratio (target gene/CD31 gene)			
		Flt-1	Flk-1	Tie1	Tie2
MDA-MB-231	Control	0.22 ± 0.02	0.80 ± 0.07	0.56 ± 0.10	0.10 ± 0.01
	SQMG 5	0.22 ± 0.02	0.82 ± 0.06	0.59 ± 0.06	0.07 ± 0.01
	SQMG 20	0.26 ± 0.04	0.69 ± 0.06	0.64 ± 0.01	0.06 ± 0.02**
A549	Control	0.21 ± 0.01	0.82 ± 0.02	0.64 ± 0.09	0.20 ± 0.01
	SQMG 5	0.20 ± 0.01	0.67 ± 0.02	0.58 ± 0.10	0.08 ± 0.01**
	SQMG 20	0.24 ± 0.01	0.79 ± 0.01	1.21 ± 0.38*	0.14 ± 0.012*
WiDr	Control	0.33 ± 0.02	0.69 ± 0.02	0.58 ± 0.03	0.08 ± 0.01
	SQMG 5	0.31 ± 0.03	0.64 ± 0.01	0.59 ± 0.02	0.07 ± 0.01
	SQMG 20	0.33 ± 0.01	0.64 ± 0.02	0.63 ± 0.02	0.06 ± 0.01*
SAS	Control	0.36 ± 0.01	1.04 ± 0.02	1.96 ± 0.58	0.20 ± 0.01
	SQMG 5	0.35 ± 0.02	0.93 ± 0.05	2.16 ± 0.73	0.18 ± 0.01
	SQMG 20	0.25 ± 0.01	0.52 ± 0.03**	1.94 ± 0.43	0.11 ± 0.01**
PC-3	Control	0.16 ± 0.01	0.93 ± 0.02	1.42 ± 0.03	0.08 ± 0.01
	SQMG 5	0.11 ± 0.13	0.73 ± 0.06	1.26 ± 0.17	0.07 ± 0.05
	SQMG 20	0.15 ± 0.02	0.78 ± 0.07	1.40 ± 0.04	0.09 ± 0.01
TE-8	Control	0.34 ± 0.03	0.74 ± 0.05	0.43 ± 0.11	0.08 ± 0.01
	SQMG 5	ND	ND	ND	ND
	SQMG 20	0.30 ± 0.02	0.70 ± 0.04	0.44 ± 0.11	0.10 ± 0.01
LU65	Control	0.23 ± 0.02	0.55 ± 0.06	0.43 ± 0.01	0.04 ± 0.01
	SQMG 5	ND	ND	ND	ND
	SQMG 20	0.21 ± 0.21	0.69 ± 0.01	0.42 ± 0.02	0.04 ± 0.01

Data are presented as mean ± SE. ND, not done; SQMG 5, treatment of 5 mg/kg SQMG; SQMG 20, treatment of 20 mg/kg SQMG.
*P < 0.05. **P < 0.01.

Fig. 6. Angiogenic receptor gene expression on capillary-formed human umbilical vein endothelial cells (HUVEC) *in vitro*. Total RNA of capillary-formed HUVEC was assessed as to the amount of mRNA copy number of human (a) *Flt-1*, (b) *KDR*, and (c) *Tie2* by quantitative real-time reverse transcription–polymerase chain reaction analysis. Results represent means ± SE of triplicate wells on one of three independent experiments.

effects of SQMG could be attributed to the inhibition of tumor angiogenesis. To analyze this mechanism, we first investigated the influence of endothelial cell proliferation and apoptosis *in vitro* by SQMG. Although the proliferation of HUVEC cells treated with 50 µM SQMG was inhibited, the apoptosis of these cells were not clearly observed. Consequently, our study implied that the inhibitory effects of SQMG shown in the MTT assay are attributed to a slower proliferation of HUVEC cells but not apoptosis.

Thus, SQMG appears to have only a weak inhibitory effect on cell proliferation and apoptosis activity as compared with other chemotherapeutic compounds for cancer.[24,25] However, the capillary formation, consisting of HUVEC treated with 50 µM SQMG, was significantly reduced approximately 70% as compared with the control. As *Tie2* but not *Flt-1* and *KDR* gene expression in capillary-formed HUVEC was decreased selectively, it is possible that some synergistic effects between slow proliferation

and downregulation of *Tie2* gene expression exist. This was comparable with our observation that xenografted tumors treated with SQMG showed downregulation of *Tie2* gene expression in the endothelial cells. In addition, we recently found that the SQMG-derivative α-SQMG (c18:0) binds to the extracelluar domains of Tie2 using phage display screening and surface plasmon resonance analysis (Sakimoto I, Ohta K, Yamazaki T, *et al.* 2006 unpublished data in Discussion of[21]). Such binding may influence antiangiogenesis through downregulation of Tie2.

The receptor tyrosine kinase Tie2 is highly expressed in endothelial cells, and plays a critical role in normal vascular development via the regulation of vascular remodeling and endothelial cell interactions with supporting pericytes and smooth muscle cells.[26–32] In particular, Tie2 is essential for the development of embryonic vasculature but not hematopoietic cell development[33] because *Tie2*^{−/−} mice die between embryonic days 9.5 and 12.5 due to lack of remodeling of the primary capillary plexus.[28,29] However, Tie2 is constitutively expressed and phosphorylated at a low level in adult mice, suggesting that Tie2 activation is required in adult tissue to maintain the mature quiescent phenotype of vasculature.[34] Interruption of Tie2 signaling with a soluble receptor can significantly inhibit tumor growth in mice, suggesting that Tie2 is important for tumor angiogenesis as well.[11] However, the molecular mechanism by which SQMG induces the downregulation of *Tie2* gene expression *in vivo* and *in vitro* was not demonstrated. The regulatory mechanism of *Tie2* gene expression by SQMG is currently under investigations.

We also observed increased *Ang1* gene expression in three of the four SQMG-sensitive tumors. Ang1 and Ang2 are known to function as ligands for Tie2. Ang1, mainly secreted from pericytes, acts as an agonist of Tie2, whereas Ang2, mainly secreted from endothelial cells, is known to act as an antagonist as well as an agonist, depending on the experimental system.[10] Ang1 specifically induces tyrosine phosphorylation of Tie2, which results in multiple activities related to angiogenesis such as endothelial cell migration,[35] tube formation,[15] sprouting,[36,37] and survival[38,39] but not proliferation of endothelial cells *in vitro*.[40] Thus, Ang1 basically act as a factor of angiogenesis. However, it was reported that Ang1-overexpressing human tumor xenografts could not grow due to inhibition of angiogenesis,[41,42] proposing an inhibitory mechanism whereby the antiangiogenic effects of Ang1 overexpression are mediated in part by increased support by vascular pericytes that results in overall vessel stabilization and therefore inhibition of the initiation of tumor angiogenesis. In the current study, although an upregulation of Ang1 in SQMG-treated tumor xenograft was observed, it remains undefined whether Tie2 phosphorylation levels were influenced by SQMG. The further regulatory mechanism of antiangiogenesis between the Ang1 and Tie2 molecules and how SQMG regulates this needs further study.

In conclusion, as little is known about chemical compounds inducing downregulation of Tie2, SQMG could be a promising candidate for the treatment of tumor-induced angiogenesis targeting Tie2.

Acknowledgments

References

1 Folkman J. What is the evidence that tumor are angiogenesis dependent? *J Natl Cancer Inst* 1990; **82**: 4–6.

2 Carmeliet P. Angiogenesis in life, disease and medicine. *Nature* 2005; **438**: 932–6.
3 O'Reilly MS, Holmgren L, Shing Y *et al.* Angiostatin: a novel angiogenesis inhibitor that mediates the suppression of metastases by a Lewis lung carcinoma. *Cell* 1994; **79**: 315–28.

Mori *et al.*

4 O'Reilly MS, Boehm T, Shing Y *et al*. Endostatin: an endogenous inhibitor of angiogenesis and tumor growth. *Cell* 1997; **88**: 277–85.

5 Fong TA, Shawver LK, Sun L *et al*. SU5416 is a potentand selective inhibitor of vascular endothelial growth factor receptor (Flk-1/KDR) that inhibits tyrosine kinase catalysis, tumor vascularization, and growth of multiple tumor types. *Cancer Res* 1999; **59**: 99–106.

6 Ferrara N, Gerber HP, LeCouter J. The biology of VEGF and its receptors. *Nat Med* 2003; **9**: 669–76.

7 Hurwitz H, Feherenbacher L, Novotny W *et al*. Bevacizumab plus irinotecan, fluorouracil, and leucovorin for metastatic colorectal cancer. *N Engl J Med* 2004; **350**: 2335–42.

8 Gerber HP, Ferrara N. Pharmacology and pharmacodynamics of bevacizumab as monotherapy or in combination with cytotoxic therapy in preclinicals studies. *Cancer Res* 2005; **65**: 671–80.

9 Ferrara N, Kerbel RS. Angiogenesis as a therapeutic target. *Nature* 2005; **438**: 967–74.

10 Eklund L, Olsen BR. Tie receptors and their angiopoietin ligands are context-depedent regulators of vascular remodeling. *Exp Cell Res* 2006; **312**: 630–41.

11 Lin P, Polverini P, Dewhirst M, Shan S, Roao PS, Peters KG. Inhibition of tumor angiogenesis using a soluble receptor establishes a role for Tie-2 in pathologic vascular growth. *J Clin Invest* 1997; **100**: 2072–8.

12 Lin P, Buxton JA, Acheson A *et al*. Anti-angiogenic gene therapy targeting the endothelium-specific receptor tyrosine kinase Tie2. *Proc Natl Acad Sci USA* 1998; **95**: 8829–34.

13 Siemeister G, Schirner M, Weindel K *et al*. Two independent mechanisms essential for tumor angiogenesis: inhibition of human melanoma xenograft growth by interfering with either the vascular endothelial growth factor receptor pathway or the Tie-2 pathway. *Cancer Res* 1999; **59**: 3185–91.

14 Stratmann A, Acker T, Burger AM, Amann K, Risau W, Plate KH. Differential inhibition of tumor angiogenesis by Tie2 and vascular endothelial growth factor receptor-2 dominant-negative receptor mutants. *Int J Cancer* 2001; **91**: 273–82.

15 Hayes AJ, Huang WQ, Mallah J, Yang D, Lippman ME, Li LY. Angiopoietin-1 and its receptor Tie-2 participate in the regulation of capillary-like tubule formation and survival of endothelial cells. *Microvasc Res* 1999; **58**: 224–37.

16 White RR, Shan S, Rusconi CP *et al*. Inhibition of rat corneal angiogenesis by a nuclease-resistant RNA aptamer specific for angiopoietin. *Proc Natl Acad Sci USA* 2003; **100**: 5028–33.

17 Niu Q, Perruzzi C, Voskas D, Lawler J, Dumont DJ, Benjamin LE. Inhibition of Tie-2 signaling induces endothelial cell apoptosis, decreases Akt signaling, and induces endothelial cell expression of the endogenous anti-angiogenic molecule, thrombospondin-1. *Cancer Biol Ther* 2004; **3**: 402–5.

18 Tournaire R, Simon M-P, le Noble F, Eichmann A, England P, Pouyssegur J. A short synthetic peptide inhibits signal transduction, migration and angiogenesis mediated by Tie2 receptor. *EMBO Rep* 2004; **5**: 1–6.

19 Sahara H, Ishikawa M, Takahashi N *et al*. *In vivo* anti-tumour effect of 3′-sulphonoquinovosyl 1′-monoacylglyceride isolated from sea urchin (*Strongylocentrotus intermedius*) intestine. *Br J Cancer* 1997; **75**: 324–32.

20 Sahara H, Hanashima S, Yamazaki T *et al*. Anti-tumor effect of chemically synthesized sulfolipids based on sea urchin's natural sulfonoquinovo-sylmonoacylglycerols. *Jpn J Cancer Res* 2002; **93**: 85–92.

21 Sakimoto I, Ohta K, Yamazaki T *et al*. α-Sulfoquinovosylmonoacylglycerol is a novel potent radiosensitizer targeting tumor angiogenesis. *Cancer Res* 2006; **66**: 2287–95.

22 Solway J, Seltzer J, Samaha FF *et al*. Structure and expression of a smooth muscle cell-specific gene, SM22α. *J Biol Chem* 1995; **270**: 13 460–9.

23 Zhang L, Yang N, Park J *et al*. Tumor-derived vascular endothelial growth factor up-regulates angiopoietin-2 in host endothelium and destabilizes host vasculature, supporting angiogenesis in ovarian cancer. *Cancer Res* 2003; **63**: 3403–12.

24 Yamori T, Matsunaga A, Sato S *et al*. Potent antitumor activity of MS-247, a novel DNA minor grove binder, evaluated by an *in vitro* and *in vivo* human cancer cell line panel. *Cancer Res* 1999; **59**: 4042–9.

25 Dan S, Tsunoda T, Kitahara O *et al*. An integrated database of chemosensitivity to 55 anticancer drugs and gene expression profiles of 39 human cancer cell lines. *Cancer Res* 2002; **62**: 1139–47.

26 Dumont DJ, Yamaguchi TP, Conlon RA, Rossant J, Breitman ML. Tek, a novel tyrosine kinase gene located on mouse chromosome 4, is expressed in the endothelial cells and their presumptive precursors. *Oncogene* 1992; **7**: 1471–80.

27 Dumont DJ, Gradwohl GJ, Fong GH, Auerbach R, Breitman ML. The endothelial-specific receptor tyrosine kinase, tek, is a member of a new subfamily of receptors. *Oncogene* 1993; **8**: 1293–301.

28 Dumont DJ, Gradwohl G, Fong GH *et al*. Dominant-negative and targeted null mutations in the endothelial receptor tyrosine kinase, tek, reveal a critical role in vasculogenesis of the embryo. *Genes Dev* 1994; **8**: 1897–909.

29 Sato TN, Tozawa Y, Deutsch U *et al*. Distinct roles of the receptor tyrosine kinases Tie1 and Tie-2 in blood vessel formation. *Nature* 1995; **376**: 70–4.

30 Maisonpierre PC, Suri C, Jones PF *et al*. Angiopoietin-2, a natural antagonist for Tie2 that disrupts *in vivo* angiogenesis. *Science* 1997; **277**: 55–60.

31 Hanahan D. Signaling vascular morphogenesis and maintenance. *Science* 1997; **277**: 48–50.

32 Davis S, Yancopoulos GD. The angiopoietins: ying and yang in angiogenesis. *Curr Top Microbiol Immunol* 1999; **237**: 173–85.

33 Hamaguchi I, Morisada T, Azuma M *et al*. Loss of Tie2 receptor compromises embryonic stem cell-derived endothelial but not hematopoitic cell survival. *Blood* 2006; **107**: 1207–13.

34 Wong AL, Haroon ZA, Werner S, Dewhirst MW, Greenberg CS, Peters KG. Tie2 expression and phosphorylation in angiogenic and quiescent adult tissues. *Circ Res* 1997; **81**: 567–74.

35 Witzenbichler B, Maisonpierre PC, Jones P, Yancopoulos GD, Isner JM. Chemotactic properties of angiopoietin-1 and -2, ligands for the endothelial-specific receptor tyrosine kinase Tie2. *J Biol Chem* 1998; **273**: 18 514–21.

36 Koblizek TI, Weiss C, Yancopoulos GD, Deutsch U, Risau W. Angiopoietin-1 induces sprouting angiogenesis *in vitro*. *Curr Biol* 1998; **8**: 529–32.

37 Kim I, Kim HG, Moon SO *et al*. Angiopoietin-1 induces endothelial cell sprouting through the activation of focal adhesion kinase and plasmin secretion. *Circ Res* 2000; **86**: 952–9.

38 Kim I, Kim HG, So JN, Kim JH, Kwak HJ, Koh GY. Angiopoietin-1 regulates endothelial cell survival through the phosphatidylinositol 3V-kinase/Akt signal transduction pathway. *Circ Res* 2000; **86**: 24–9.

39 Daly C, Wong V, Burova E *et al*. Angiopoietin-1 modulates endothelial cell function and gene expression via the transcription factor FKHR (FOXO1). *Genes Dev* 2004; **18**: 1060–71.

40 Davis S, Aldrich TH, Jones PF *et al*. Isolation of angiopoietin-1, a ligand for the TIE2 receptor, by secretion-trap expression cloning. *Cell* 1996; **87**: 1161–9.

41 Hawighorst T, Skobe M, Streit M *et al*. Activation of the tie2 receptor by angiopoietin-1 enhances tumor vessel maturation and impairs squamous cell carcinoma growth. *Am J Pathol* 2002; **160**: 1381–92.

42 Stoeltzing O, Ahmad SA, Liu W *et al*. Angiopoietin-1 inhibits vascular permeability, angiogenesis, and growth of hepatic colon cancer tumors. *Cancer Res* 2003; **63**: 3370–7.

Gene Expression Profile of Dorsal Root Ganglion in a Lumbar Radiculopathy Model

Hirohito Takeuchi, MD,* Satoshi Kawaguchi, MD,* Satoshi Mizuno, MD,*
Takashi Kirita, MD,* Tsuneo Takebayashi, MD,* Kumiko Shimozawa, MSc,†
Toshihiko Torigoe, MD,‡ Noriyuki Sato, MD,‡ and Toshihiko Yamashita, MD*

Study Design. DNA array analysis of dorsal root ganglion (DRG) using a rat model with nerve root constriction.

Objective. To determine the molecular changes in the DRG adjacent to the injured nerve root in a lumbar radiculopathy model.

Summary of Background Data. DNA array analysis in lumbar radiculopathy model has so far focused on the spinal dorsal horn. The molecular changes in the DRG adjacent to the injured nerve root in lumbar radiculopathy remain to be determined.

Methods. Bilateral L5 DRGs were removed from 12 Sprague-Dawley rats on days 2, 7, 14, and 21 after nerve root ligation and on day 7 from 3 rats with sham operation. The aRNAs from the DRGs with nerve root ligation were labeled with Cy5 dye and those from the opposite side DRG (control) were labeled with Cy3 dye, and then hybridized to a 7793-spot Panorama Micro Array. It was considered to be significantly upregulated, when an average expression ratio of Cy5 to Cy3 was 2 or more. Genes upregulated were classified into early phase group (upregulated on day 2), midphase group (upregulated on days 7 and 14), and continuous group (upregulated from day 2 to 21). Seventeen genes were subjected to validation analysis with real-time quantitative PCR.

Results. There were 16 upregulated genes in the early phase group, 56 genes in the midphase group, and 17 genes in the continuous group. Functional categorization revealed dominantly upregulated gene categories in each group; transcription/translation in the early phase group, enzyme/metabolism in the midphase group, and structure in the continuous group. Validation analysis of 17 genes demonstrated mean relative expression of 2.0 or more in all but 1 gene in the DRGs with nerve root ligation and none of them in the DRGs with sham operation.

Conclusion. The genes identified in this study, especially those involved in pain signaling and inflammation, serve as potential targets for molecular-based therapy for lumbar radiculopathy.

Key words: cDNA microarray, Sprague-Dawley rats, dorsal root ganglion, nerve root ligation, lumbar radiculopathy. **Spine 2008;33:2483–2488**

Painful lumbar radiculopathy is a common, disabling condition associating with disc herniation and spinal stenosis in the lumbar spine.[1,2] In addition to mechanical compression of nerve roots, subsequent molecular events in the adjacent dorsal root ganglion (DRG) and the dorsal horn of the spinal cord play a crucial regulatory role in the severity and chronicity of lumbar radicular pain.[3,4]

With the emergence of high-density DNA array technology, it has become possible to comprehensively investigate the levels of mRNA transcripts in tissues.[5,6] In peripheral nerve injury models, a number of DNA array studies have analyzed changes in mRNA transcripts in the DRG[7–10] and the spinal dorsal horn.[11–13] In contrast, DNA array analysis in lumbar radiculopathy model has so far focused on the spinal dorsal horn.[4,14] The molecular changes in the DRG adjacent to the injured nerve root in lumbar radiculopathy remain to be determined.

In the present study, the authors used DNA array technology in a rat model[15] to determine the gene profile in the DRG adjacent to the injured nerve root.

■ Materials and Methods

Animal Model

Sprague-Dawley rats (6-week-old males) were maintained in a climate-controlled room on a 12/12 hours day/night cycle and allowed free access to food and water. All animal care and experiments were carried out according to the protocol approved by the Institutional Animal Care Committee of Sapporo Medical University, Sapporo, Japan. The lumbar nerve root ligation model was developed previously in our laboratory[15] by modifying a reported model.[16] Briefly, under anesthesia with intraperitoneal injection of sodium pentobarbital (50 mg/kg body weight), the L5 lamina was removed. The left L5 nerve root was isolated and tightly ligated using a 8 to 0 nylon suture proximal to the DRG. In sham-operated rats, the right L5 nerve root was exposed by laminectomy without ligation.

Manifestation of neuropathic pain of these rats was evaluated by their susceptibility to mechanical stimuli before RNA preparation from the DRG as described previously.[15] Rats were subjected to sequential series of tactile stimulations to the plantar surface of the ipsilateral (nerve root ligated) hind paw using 12 g von Frey filaments (Stoelting, IL). The mechanical stimulus was applied to the middle area between the foot pads on the plantar surface of the left (constriction side) and right (contralateral side) hind paw. Each hind paw was probed con-

secutively with 10 tactile stimulations alternating between the left and right. The trial was repeated successively 3 times with at least a 10-minute interval, which resulted in each foot receiving 30 mechanical stimulations. Mechanical sensitivity was assessed by counting the total number of withdrawal responses elicited for a total possible score of 30. Therefore, the mechanical withdrawal frequency of each rat was expressed as the number of responses obtained from the contralateral side (no constricted) was subtracted from the number of responses from the ipsilateral or constricted side. Preliminary experiments confirmed the reproducibility of pain behavior in the model. Some rats having undergone ligation of the L5 root showed plantar-flexed toe deformity in the ipsilateral hind paw, which improved within 2 weeks. None of the model rats showed gait disturbance or drop foot. Subsequent to the preliminary experiments, the rats showing allodynic responses (5 times or more of subtracted withdrawals on day 2 after the operation) were elected for subsequent RNA preparation.

RNA Preparation and Labeling

Bilateral L5 DRGs were removed from rats on day 2, 7, 14, and 21 after nerve root ligation and on day 7 from sham-operated rats. Three rats were used on each day and were designated a, b, and c, respectively. They were stored at $-80°C$ until use. Total RNAs were extracted from DRG samples with an RNeasy Mini Kit (Qiagen, Valencia, CA), according to the manufacturer's protocol. The quality of RNA was assessed by electrophoresis on 1.5% agarose gel.

Using an Amino Allyl MessageAmp aRNA Kit (Ambion, Austin, TX), total RNAs from DRGs were reverse transcribed to single-strand cDNA with the oligo-dT primer containing a T7 promoter sequence. The single-strand cDNA was then converted into a double-strand cDNA template with the T7 promoter primer. Multiple copies of amino allyl-modified aRNA were generated from the double-strand cDNA templates with aaUTP. The aRNAs from the DRGs with nerve root ligation were labeled with Cy5 dye and those from the opposite side DRG (control) were labeled with Cy3 dye.

Hybridization to cDNA Microarrays and Data Analysis

The dye-labeled aRNA samples were hybridized to a 7793-spot Panorama Micro Array (Sigma Genosys, Ishikari, Japan) for 16 hours at 45°C. One array membrane was used for each experimental rat. Intensity of Cy3 and Cy5 fluorescence for every gene spot on hybridized arrays was measured with a GenePix 4000B scanner (Axon Instrument, Austin, TX), and was analyzed with GenePix Pro 5.0 software (Axon Instrument).

For normalization, the fluorescent ratio for each spot was first log-transformed using TIGR MIDAS software, version 2.19 (The Institute for Genomic Research, Rockville, MD). Then the data for each sample were mean centered. Spots that could not be interpreted were excluded, resulting in a list of 7513 genes available for subsequent analysis. The average of expression ratio of Cy5 to Cy3 was obtained for each gene in triplicate microarray experiments (3 rats in the same experimental condition). The average ratio of 2 or more was determined as differentially expressed. Genes were classified into functional categories according to the categorization of Lacroix-Fralish et al.[4]

Real-Time Quantitative PCR

Seventeen genes that had been upregulated in DRG of ligated nerve roots on day 7 and also in a peripheral axotomy model in the literature[8] were picked up for validation analysis with real-
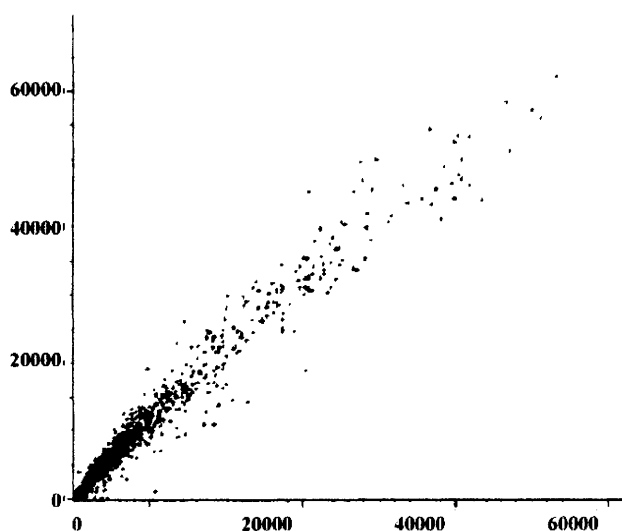

Figure 1. Scatter plot representation of lumbar DRG gene expression. Gene expression signals of the bilateral L5 DRGs in a rat 14 days after ligation of the left L5 nerve root are shown. The x-axis indicates the gene expression signals in the DRG of the ligated left L5 nerve root. The y-axis indicates the gene expression signals of the DRG of the right L5 nerve root (opposite side).

time quantitative PCR. TaqMan probes for these 17 genes were designed by and purchased from Applied Biosystems (Foster City, CA). Total RNA was extracted from bilateral L5 DRGs of nerve root-ligated rats (n = 3) and sham-operated rats (n = 3) on day 7 after surgery and reverse transcribed as described earlier. For individual reactions, 1 μg of each sample cDNA was combined with 25 μL of TaqMan Universal PCR Master Mix, 2.5 μL of Inventoried Gene Expression Assay Mix including TaqMan probe, 1.5 μL of GAPDH Control Mix, and 20 μL of RNase-free water. Real-time PCR was performed with the ABI PRISM 7000 Sequence Detection system (Applied Biosystems) according to the manufacturer's protocol. All amplifications were done in triplicate and threshold cycle (C_t) scores were averaged for subsequent calculations of relative expression values. The C_t scores represent the cycle number at which fluorescence signal crosses an arbitrary threshold. The C_t scores of genes of interest for each sample were normalized against C_t scores of GAPDH. Relative expression of genes in the DRG with nerve root ligation/sham operation versus those in the opposite side DRG (control) was determined by the following calculation: Relative expression = $2^{-\Delta\Delta C_t}$ where $\Delta\Delta C_t$ = (C_t of ligated/sham-operated nerve DRG $-$ C_t of GAPDH) $-$ (C_t of control DRG $-$ C_t of GAPDH). The mean of relative expression for each sample from 3 rats was then calculated.

■ Results

Cluster Analysis of Gene Expression Profiles of DRG Samples

To establish gene expression profiles of a lumbar radicular pain model, we carried out cDNA array analysis on DRG sample pairs from 12 different rats with lumbar nerve root ligation and 3 rats with sham operation. As representatively shown in Figure 1, the expression of most lumbar DRG genes was not strongly changed after ligation of the nerve root. We then subjected the expression profiles of the 15 DRG sample pairs to a hierarchical
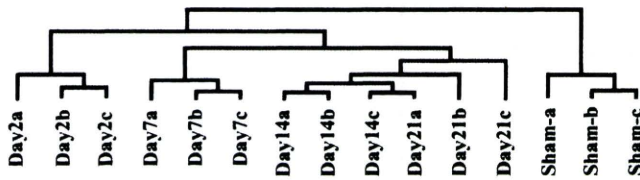
Figure 2. Hierarchial clustering of the expression profiles of 15 DRG sample pairs.

clustering analysis (Figure 2). As shown, the 3 DRG samples from sham-operated rats composed a cluster. Apart from this cluster, the 12 DRG sample pairs of nerve root-ligated rats were clustered into one large group. This group was further subdivided into 2 subgroups; 1 composed of the day-2 DRG samples, and the other composed of day-7, day-14, and day-21 samples.

Identification of Upregulated Genes in the DRG Adjacent to the Ligated Nerve Root

Based on the clustering analysis, we subsequently defined genes that were upregulated at day 2 after nerve root ligation (early phase group) and those upregulated at days 7 and 14 (midphase group). We also defined genes that were continuously upregulated from day 2 to day 21 after nerve root ligation (continuous group). As depicted in Table 1, sixteen genes were upregulated in the DRG specifically at day 2 after nerve root ligation. There were 56 genes that were upregulated both at day 7 and day 14, but not day 2 (Table 2). Seventeen genes were continuously upregulated from day 2 to day 21 after nerve root ligation (Table 3). Thus, upregulation of genes was most active in the midphase in line with the painful behavior of rats that peaked during this phase.[15]

We then classified genes into 9 functional categories. Table 4 summarizes the percentages of categorized genes in the early phase, midphase, and continuous groups. Genes categorized into cell cycle, channels/transporters, growth factors/cytokines, and synaptic represented less than 10% of the upregulated genes in all 3 groups. In

contrast, 31% of genes were categorized into transcription/translation in the early phase, whereas there were 15% in the midphase and 0% in the consistent group. Inversely, more genes were involved in enzyme/metabolism and structure in the midphase and continuous groups than in the early phase group. Genes involved in signal transduction comprised 19% and 20% of the upregulated genes in the early phase and the midphase, respectively.

Validation Analysis of Array Results

Finally we evaluated the validity of array results by real-time quantitative RT-PCR. Seventeen genes were picked up from 56 genes in the midphase group. Relative expression of these genes was determined in DRGs with nerve root ligation and those with sham operation on day 7, respectively. As depicted in Table 5, all but opioid growth factor receptor showed mean relative expression of 2.0 or more in the DRGs with nerve root ligation by real-time quantitative RT-PCR. In contrast, mean relative expression of 17 genes was 1.3 or lower in the DRGs with sham operation.

■ Discussion

In the present study, we analyzed the gene expression profile of DRG neurons using a cDNA microarray in a rat nerve root ligation model. This model was used in our previous electrophysiological analysis of the DRG neurons as a lumbar radiculopathy model,[15] showing behavioral data consistent with those in the original model.[16,17] The present study was designed to extend the electrophysiological approach toward comprehensive gene profiling. We found, by cluster analysis of triplicate microarray experiments, that the gene expression profiles were distinct, with 1 set of DRG samples in sham-operated rats and another in rats having undergone nerve root ligation. In addition, among the 12 DRG samples in rats with ligated nerve roots, the 9 DRG samples taken at day 7, 14, and 21 were clustered into 1 group, apart from a

Table 1. List of DRG Genes Selectively Upregulated at Day 2 After Nerve Root Ligation

Gene Symbol	Gene Name	Accession No.	Functional Categorization	Day 2	Day 7	Day 14
Aurkb	Aurora kinase B	D89731	Cell cycle	2.2	1.6	1.5
CLCA	Putative calcium-activated chloride channel	AF077303	Channels/transporters	7.2	0.8	0.9
Ptgs2	Prostaglandin-endoperoxide synthase 2	NM_017232	Enzyme/metabolism	3.9	1.2	1.4
Hmox1	Heme oxygenase (decycling) 1	NM_012580	Enzyme/metabolism	2.6	1.6	1.1
Scgb1a1	Secretoglobin, family 1A, member 1	NM_013051	Growth factors/cytokines	2.0	1.3	1.2
Daf1	Decay accelarating factor 1	AF039584	Immune	2.1	1.4	1.6
Prlr	Prolactin receptor	L48060	Signal transduction	2.1	1.5	1.3
Nrcam	Neuron-glia-CAM-related cell adhesion molecule	U81037	Signal transduction	2.0	1.2	1.1
Flot2	Flotillin 2	AF023302	Signal transduction	2.0	1.5	1.6
Adcyap1	Adenylate cyclase activating polypeptide 1	NM_016989	Synaptic	2.8	1.6	1.4
Fosl1	Fos-like antigen 1	NM_012953	Transcription/translation	2.3	1.6	1.2
Ncl	Nucleolin	NM_012749	Transcription/translation	2.1	1.9	1.6
Rplp1	Ribosomal protein, large, P1	X15097	Transcription/translation	2.1	1.7	1.4
Pabpc1	Poly(A) binding protein, cytoplasmic 1	NM_134353	Transcription/translation	2.1	1.5	1.9
Rbm3	RNA binding motif (RNP1, RRM) protein 3	AF355190	Transcription/translation	2.0	1.8	1.5
Sval1	Seminal vesicle antigen-like 1	NM_133292	Unknown	2.0	0.7	0.8

The average Cy5/Cyt 3 ratio of gene in triplicate microarray experiments were calculated. Genes showing the ratio of 2 or more at day 2, but not at day 7 and day 14 were listed.